



# Estimating reservoir evaporation losses for the United States: Fusing remote sensing and modeling approaches

Gang Zhao, Huilin Gao\*

Zachry Department of Civil Engineering, Texas A&M University, College Station, TX 77843, USA

## ARTICLE INFO

### Keywords:

Evaporation  
Heat storage  
Landsat  
Water mapping  
Brightening

## ABSTRACT

Evaporation from open surface water is a critical and continuous process in the water cycle. Globally, evaporation losses from reservoirs are estimated to be greater than the combined consumption from industrial and domestic water uses. However, this large volume of water loss is only coarsely considered in modern water resources management practices due to the complexities involved with quantifying these losses. By fusing remote sensing and modeling approaches, this study developed a novel method to accurately estimate the evaporation losses from 721 reservoirs in the contiguous United States (CONUS). Reservoir surface areas were extracted and enhanced from the Landsat based Global Surface Water Dataset (GSWD) from March 1984 to October 2015. The evaporation rate was modeled using the Penman Equation in which the lake heat storage term was considered. Validation results using in situ observations suggest that this approach can significantly improve the accuracy of the simulated monthly reservoir evaporation rate. The evaporation losses were subsequently estimated as the product of the surface area and evaporation rate. This paper presents a first of its kind, comprehensively validated, locally practical, and continentally consistent reservoir evaporation dataset. The results suggest that the long term averaged annual evaporation volume from these 721 reservoirs is  $33.73 \times 10^9 \text{ m}^3$ , which is equivalent to 93% of the annual public water supply of the United States (in 2010). An increasing trend of the evaporation rate ( $0.0076 \text{ mm/d/year}$ ) and a slightly decreasing trend of the total surface area ( $-0.011 \times 10^9 \text{ m}^2/\text{year}$ ) were both detected during the study period. As a result, the total evaporation shows an insignificant trend, yet with significant spatial heterogeneity. This new reservoir evaporation dataset can help facilitate more efficient water management practices.

## 1. Introduction

It has been projected that 5.3 billion people will live under water stress and water scarcity globally by 2030 (Organisation for Economic Co-operation and Development, 2008). Most of the affected population relies on surface water—especially the water impounded by reservoirs, which can be easily accessed and managed (United Nations Environment Programme, 2013). In addition to supplying water for agricultural, municipal, and industrial uses, reservoirs can also be used for flood control and hydropower generation. From 1950 to 2007, the cumulative volume of water impounded by global reservoirs rose from about  $1000 \text{ km}^3$  to  $11,000 \text{ km}^3$ , reducing the global sea level rise by 30 mm (Chao et al., 2008). According to the Global Reservoir and Dam Database (GRanD; Lehner et al., 2011), the United States is the country with the largest number of reservoirs. These reservoirs are capable of storing  $1300 \text{ km}^3$  of water, which is almost equivalent to the region's annual mean runoff (Graf, 1999).

Globally there are about 16.7 million reservoirs that have a surface area of  $100 \text{ m}^2$  or greater (Lehner et al., 2011). These reservoirs have increased the global terrestrial water surface area by about  $305,000 \text{ km}^2$ . With the large amount of surface area that is produced by these artificial impoundments, the evaporative loss is significant—especially in semi-arid and arid regions (Ali et al., 2008; Morton, 1979). For example, the annual evaporation loss from 200 reservoirs in Texas, USA, equals to 20% of their active storage (Zhang et al., 2017). The long-term evaporation from Lake Tahoe, which is located in the arid western United States, accounts for 40%–60% of the total reservoir output (Friedrich et al., 2018). The reservoir evaporation of Lake Mead ( $\sim 1800 \text{ mm/year}$ ; Moreo, 2015) is much larger than the surrounding evapotranspiration ( $\sim 50 \text{ mm/year}$ ; Mu et al., 2011), which can be regarded as pre-reservoir ET. From a global perspective, Shiklomanov (1999) estimated a total of  $\sim 270 \text{ km}^3/\text{year}$  of reservoir evaporation, which is larger than the combined domestic and industrial water use in the year 2010 ( $\sim 250 \text{ km}^3$ ). Therefore, to better support

\* Corresponding author at: Zachry Department of Civil Engineering, Texas A&M University, College Station, TX 77843-3136, USA.  
E-mail address: [hgao@civil.tamu.edu](mailto:hgao@civil.tamu.edu) (H. Gao).

<https://doi.org/10.1016/j.rse.2019.03.015>

Received 9 November 2018; Received in revised form 7 March 2019; Accepted 10 March 2019

Available online 09 April 2019

0034-4257/ © 2019 Elsevier Inc. All rights reserved.

efficient water resources management, it is essential to incorporate accurate reservoir evaporation information into current reservoir operation rules.

Despite the critical need for reservoir evaporation information, no continentally consistent and locally practical evaporation dataset has been produced that can be used in the policy making process at a regional scale. To precisely quantify the evaporation losses from a given reservoir, water surface area and evaporation rate data are needed. However, both high quality reservoir surface area and evaporation rate data can be difficult to gather.

Reservoir surface area is usually inferred from in-situ measurements, or estimated from remote sensing images. By applying in-situ measured reservoir elevation values to a known elevation-area relationship, a reservoir's area can be calculated. The elevation-area relationship is typically derived from bathymetry investigations (either before or after the reservoir is constructed) using sonar/laser and GIS technologies. However, this method is limited by its large expense and the changes of reservoir bathymetry due to sedimentation. Remote sensing has the advantage of estimating water surface area from satellite images at low cost (McFeeters, 1996; Sawaya et al., 2003; Gao, 2015). Even though there is always a compromise between spatial and temporal resolution with remote sensing technologies, usually high quality images with acceptable time intervals can be obtained. Compared with other remote sensing data, Landsat has the advantages of long temporal coverage and high spatial resolution, which makes it suitable for water surface area change studies (Pekel et al., 2016; Donchyts et al., 2016; Khandelwal et al., 2017). However, a major limitation of using Landsat images for continuous water area monitoring is the frequent contamination from multiple sources, such as clouds, cloud shadows, terrain shadows, and the Scan Line Corrector (SLC) failure (for Landsat 7). As a result, direct water extraction from the contaminated satellite images can lead to significant underestimation. To generate reliable water area estimates, most studies have simply removed the contaminated images. For instance, Busker et al. (2018) removed all of the images which are > 5% contaminated to get the surface area time series for 135 global lakes. However, this has led to many missing values in the time series, especially for the regions that have frequent cloud coverage. To bridge this gap, Zhao and Gao (2018) developed an image enhancement algorithm to automatically repair the contaminated reservoir images extracted from the Global Surface Water Dataset (GSWD; Pekel et al., 2016). The new algorithm resulted in a Global Reservoir Surface Area Dataset (GRSAD), which significantly improved the continuity of the reservoir area time series (i.e., 81% improvement on a global scale).

The evaporation rate of open water has been studied for decades. Comprehensive reviews of evaporation rate estimation methods can be found in Morton (1994) and the more recently Friedrich et al. (2018). The pan evaporation method has been employed by the National Weather Service (NWS) for estimating the point evaporation rate operationally for many decades. In addition to the primary purpose of assessing the spatial variability of atmospheric evaporative demand (AED) for irrigation scheduling, the pan evaporation data are also used for other applications such as investigating climate change and estimating reservoir evaporation (Stanhill, 2002; Ohmura and Wild, 2002; Rotstayn et al., 2006). Although there are about 950 pan evaporation stations across the CONUS, only a very small portion of these are located close enough to dams to estimate reservoir evaporation. Furthermore, lake evaporation estimation based on pan evaporation is subject to large errors due to multiple factors. These include ignoring the microclimate difference between the reservoir and the pan, not accounting for heat storage effects, extra heat absorption from the pan's sides, water splashing, overflow due to intensive rainfall, freezing conditions, human error, and others (McMahon et al., 2013; Friedrich et al., 2018). Thus, it is regarded as one of the least accurate evaporation estimation methods and is not suitable for precise water management practices (Tanny et al., 2008; Harwell, 2012; McJannet

et al., 2017). In addition to the pan evaporation method, eddy covariance (EC), scintillometer, mass balance, Bowen ratio energy budget (BREB), and combination equation methods are frequently used. In general, EC is considered the most accurate approach—but it has been primarily used for evapotranspiration related research. Constrained by the expensive cost and the sensitivity to wind direction (relative to both sensor and reservoir location), very few lake evaporation data have been collected using this approach. By measuring the sensible heat flux, a scintillometer can estimate the latent heat flux if other energy terms are known, even though it has multiple limitations (such as signal saturation) (Moene et al., 2009). The mass balance and BREB methods are both data intensive. Mass balance requires inputs of inflow (tributary + lateral), outflow (outlet + lateral), storage change, and water use data. The BREB method requires measuring heat storage changes and water surface temperatures, in addition to other meteorological forcings (Morton, 1986; Morton, 1994). Both methods can result in considerable error introduced by the complex inputs (Stannard et al., 2013; Friedrich et al., 2018).

Among the various approaches for estimating the evaporation rate on a large scale, the most practical one involves using a physically based combination equation such as the Penman equation (Penman, 1948). Some variants include PenPan (Rotstayn et al., 2006; for estimation of pan evaporation), Penman-Monteith (Monteith, 1965; commonly used for potential evapotranspiration estimation), and the Priestley-Taylor equations (Priestley and Taylor, 1972; for quantifying wet-surface evaporation in advection-free conditions). The PenPan equation has the same form as the Penman equation but includes different parameterizations. The Penman-Monteith equation introduced physically based aerodynamic resistance to replace the empirical wind function. For the Priestley-Taylor equation, an empirical coefficient ( $\alpha_{PT} = 1.26$ ) was used to approximate the aerodynamic term in the Penman equation. The value 1.26 was found to be appropriate for non-advective conditions but may change under advective conditions (Assouline et al., 2016; Eichinger et al., 1996; Flint and Childs, 1991). Detailed comparisons of these methods can be found in McMahon et al. (2013) and Wang and Dickinson (2012). These physically based models are proven to be reliable for applications over shallow water reservoirs (typically < 3 m in depth) where heat storage is insignificant (Abtew, 2001; Linacre, 1993; Zhao et al., 2016). However, lakes and reservoirs usually have a considerable heat storage effect, causing combination equations to be biased with regard to seasonal evaporation rate estimation (Finch and Hall, 2001; McMahon et al., 2013). For example, in Lake Tahoe (California, US), the air temperature is highest in July, but the largest evaporation rate occurs in September (Tahoe Environmental Research Center, 2015). To address this issue, Edinger et al. (1968) introduced the equilibrium water temperature, and de Bruin (1982) incorporated it into evaporation rate estimation. The equilibrium temperature is the water temperature at which there is no heat exchange between the air and water under constant forcings. It can help calculate the water column temperature and (then) the heat storage changes. This concept has been used in several studies, and has proven to be appropriate for open-water evaporation estimation (Finch, 2001; Finch and Hall, 2001; Bogan et al., 2003; Caissie et al., 2005; McJannet et al., 2008; Mekonnen and Hoekstra, 2012). Although the derivations of the equilibrium temperature in these studies were all based on the energy balance of the water body, different studies have adopted different simplified energy terms. For instance, the most generic form of the equilibrium temperature was from Mohseni and Stefan (1999), which used a simplified latent heat flux formulation. Therefore, there is a lack of a generalized formulation of the equilibrium temperature to improve upon the open-water evaporation estimation using the Penman equation.

Therefore, this study focuses on breaking the above key barriers in reservoir evaporation quantification to better support more precise water resources management at both local (individual reservoir) and regional (multiple reservoirs) scales. A total of 721 reservoirs, which

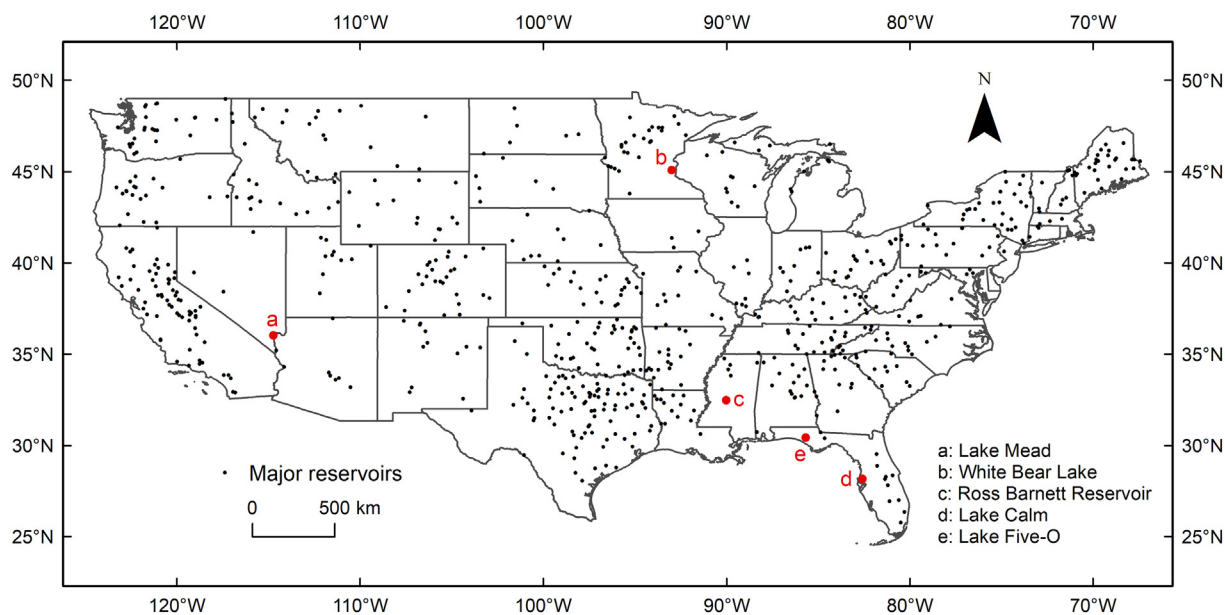


**Fig. 1.** The 721 reservoirs over the CONUS selected in this study. The five reservoirs with EC or BREB evaporation rates were shown in red. Among these reservoirs, 718 of them are major reservoirs with a storage capacity larger than  $10^8 \text{ m}^3$ , and the remaining 3 are smaller reservoirs (but with in situ evaporation rate data available, which is used for validation purposes). (For interpretation of the references to colour in this figure legend, the reader is referred to the web version of this article.)

account for 90.2% of the large reservoir storage capacity in the CONUS (Fig. 1), were chosen as our study sites (Lehner et al., 2011). Specifically, our three objectives were to: 1) adopt continuous reservoir surface area time series generated from a Landsat-based water classification dataset that is free of image contamination; 2) quantify heat storage changes in the Penman equation to better simulate the monthly reservoir evaporation rate; 3) generate the long-term monthly evaporation volume dataset for the 721 reservoirs and analyze the long-term trends of reservoir evaporation. Even though this study focuses on reservoirs in the CONUS, the retrieval algorithms and the data analysis approaches are transferable to other regions or to a global scale. These objectives provide the structural sub-headings used in the following *Methods, Results and Discussions* sections.

## 2. Data and methods

### 2.1. Estimation of reservoir surface area

The surface area time series data for the 721 reservoirs were extracted from the Landsat based GRSAD by Zhao and Gao (2018). The dataset was built upon the GSWD, which includes the global water areas for each month from March 1984 to October 2015 (Pekel et al., 2016). By applying a complex expert system classification method (on  $\sim 3$  million Landsat images from 1984 to 2015), the GSWD generated monthly global water coverage maps at 30-meter resolution. Each 30 m by 30 m pixel was classified as open water, land, or no-data. The no-data class indicates that the pixel is covered by snow, ice, cloud, shadow, or sensor-related issues. Because these types of contamination are very common—and because Landsat 7 also suffered from SLC failure (since 2003)—a large portion of the pixels in the GSWD were assigned as no-data. As a result, the direct area extraction of open water class can result in significant underestimation of the reservoir surface area. Zhao and Gao (2018) developed an image enhancement algorithm to automatically repair the contaminated images to get the full water coverage (i.e., directly seen water area, and the water area covered by contaminated sources such as clouds). Compared with the raw time series directly extracted from the GSWD, the enhanced time series from the GRSAD has significantly improved continuity and thus is more

appropriate for evaporation volume quantification. More detailed validation results about the surface area estimations can be found in Pekel et al. (2016) and Zhao and Gao (2018).

### 2.2. Estimation of reservoir evaporation rate

#### 2.2.1. Data for calculating evaporation rate

The monthly meteorological data used for calculating the evaporation rate includes air temperature, vapor pressure deficit, wind speed, and surface shortwave radiation. These are the four primary meteorological variables governing the evaporation process (McVicar et al., 2012). To consider the uncertainties from the inputs, these variables were adopted from three long-term datasets: 1) TerraClimate ( $1/24^\circ$  spatial resolution; Abatzoglou et al., 2018); 2) North American Land Data Assimilation System phase 2 (NLDAS-2) forcings ( $1/8^\circ$ ; Xia et al., 2012); and 3) Global Land Data Assimilation System Version 2 and Version 2.1 (GLDAS-2 and GLDAS-2.1;  $1/4^\circ$ ; Rodell et al., 2004).

TerraClimate inherited the solar radiation and wind speed from the Japanese 55-year Reanalysis (JRA-55) project, while air temperature and vapor pressure were extracted from the Climate Research Unit time series data version 4.0 (CRU Ts4.0). Both JRA-55 and CRU Ts4.0 were downsampled to the TerraClimate resolution using the  $1/24^\circ$  WorldClim dataset (Abatzoglou et al., 2018). Primarily based on the North American Regional Reanalysis (NARR) dataset, NLDAS-2 combined multiple data sources—including ground and satellite data—to generate a meteorological dataset with a high temporal resolution (3-hourly). The monthly data were calculated by simply averaging the 3-hourly values. Validations against in-situ observations suggest that the NLDAS retrospective forcing data are of high quality (Luo et al., 2003; Xia et al., 2012). GLDAS-2 and GLDAS-2.1 data extend the periods from 1948 to 2010 and from 2000 to present, respectively. GLDAS-2 was generated primarily from the Princeton global meteorological dataset (Sheffield et al., 2006), while GLDAS-2.1 was driven by a set of land surface models and observation data (Rui and Beaudoin, 2011). To cover the entire period of this study (i.e., 1984 to 2015), we used data from both GLDAS-2 (from 1984 to 1999) and GLDAS-2.1 (from 2000 to 2015).

For each of the reservoirs, the forcing data time series were generated by averaging the overlapping cells from the gridded forcing data

with the reservoir shapefiles. This can help reduce the uncertainty of gridded forcing data and facilitate the usage of universal fetch for all of the cells.

### 2.2.2. Algorithm for evaporation rate

With both energy budget and mass transfer terms included, combination equations can provide precise reservoir evaporation estimation. In 1948, Penman derived the first combination equation for open water evaporation estimation (Eq. (1)):

$$E = \frac{s(R_n - \Delta U) + \gamma f(u)(e_s - e_a)}{\lambda_v(s + \gamma)} \quad (1)$$

where  $E$  is the open water evaporation rate ( $\text{mm}\cdot\text{d}^{-1}$ );  $s$  is the slope of the saturation vapor pressure curve ( $\text{kPa}\cdot\text{C}^{-1}$ );  $R_n$  is the net radiation ( $\text{MJ}\cdot\text{m}^{-2}\cdot\text{d}^{-1}$ );  $\Delta U$  is the heat storage changes of the water body ( $\text{MJ}\cdot\text{m}^{-2}\cdot\text{d}^{-1}$ );  $f(u)$  is the wind function ( $\text{MJ}\cdot\text{m}^{-2}\cdot\text{d}^{-1}\cdot\text{kPa}^{-1}$ );  $e_s$  is the saturated vapor pressure at air temperature ( $\text{kPa}$ );  $e_a$  is the air vapor pressure ( $\text{kPa}$ );  $\lambda_v$  is the latent heat of vaporization ( $\text{MJ}\cdot\text{kg}^{-1}$ ); and  $\gamma$  is the psychrometric constant ( $\text{kPa}\cdot\text{C}^{-1}$ ). The Penman equation and its variants (e.g., the Penman-Monteith equation) have been widely employed for potential evapotranspiration as well as for open water evaporation estimations (McJannet et al., 2008; Tanny et al., 2008; McMahan et al., 2013).

However, there are two key factors that need to be considered when applying the Penman equation to open water evaporation estimation. The first is associated with the meteorological data that are used to drive the Penman equation. Ideally, the meteorological data should be directly collected over the water surface. However, due to the difficulties, logistics, and costs associated with acquiring measurements over water, most studies have employed land-based meteorological data as a substitute (Winter et al., 1995; dos Reis and Dias, 1998; McJannet et al., 2012). Direct use of land-based meteorological data in the Penman equation is likely to result in a biased estimation, given the meteorological differences between land and water areas (Weisman and Brutsaert, 1973). Specifically, when air moves from land across the water body, its humidity gradually increases due to the evaporation processes on the water surface. This will lead to decreasing evaporation fluxes in the downwind direction.

To solve this problem, McJannet et al. (2012) developed a generally applicable wind function that facilitates the open-water evaporation rate calculation using standard land-based meteorology. This empirical function uses a fetch length to include the effect of air becoming moister when moving from land to water surface (Eq. (2)):

$$f(u_2) = \lambda_v(2.33 + 1.65u_2)L_f^{-0.1} \quad (2)$$

where  $f(u_2)$  is the wind function ( $\text{MJ}\cdot\text{m}^{-2}\cdot\text{d}^{-1}\cdot\text{kPa}^{-1}$ );  $u_2$  is the wind speed at the height of 2 m ( $\text{m}\cdot\text{s}^{-1}$ ); and  $L_f$  is the fetch length of the water body (m). The coefficients in Eq. (2) were identified by regressing  $u_2$  and  $L_f$  against data from 19 previously published wind functions, which represent a range of water bodies with various sizes and climate conditions (McJannet et al., 2012). Because the wind speed values from reanalysis datasets are generally reported at a 10-m height, they were converted to 2-m values using the standard grass surface roughness (Allen et al., 1998). Open water roughness was not used in order to be consistent with the generalized wind function from McJannet et al. (2012).

The fetch length was calculated for each reservoir and each month (Fig. 2). With a given wind direction (monthly dominant wind direction derived from NLDAS), the width is defined as the distance between the two reservoir-tangent lines that are parallel to the wind direction. Then fetch length was calculated by dividing the total area with the width.

The second key factor to be considered when applying the Penman equation to open water evaporation is the heat storage quantification (i.e.,  $\Delta U$  in Eq. (1)). For instance, reservoirs/lakes tend to store heat in the spring/summer and release heat in the fall/winter. Without

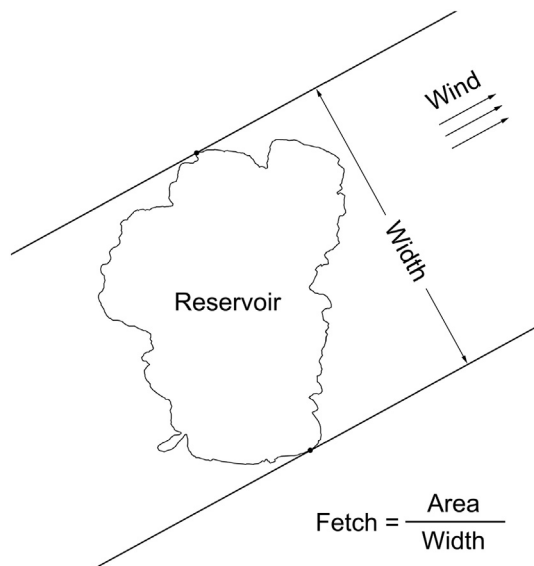


Fig. 2. Calculation of the reservoir fetch for a given wind direction.

considering this heat storage effect, the evaporation rate would be overestimated in the former and underestimated in the latter.

To represent the heat storage effect when calculating the evaporation rate, an approach using “equilibrium temperature” was adopted. The equilibrium temperature is defined as the water temperature at which there is no heat exchange between air and water (Edinger et al., 1968). If the water is under constant radiative forcing for a long enough time, the water will reach a steady state with the water temperature equal to the equilibrium temperature. In reality, the actual water temperature tends to approach the equilibrium temperature gradually. The lag time, which is defined as  $\tau$ , is dependent on the water body depth. Built upon previous studies (Edinger et al., 1968; de Bruin, 1982; Mohseni and Stefan, 1999; McMahan et al., 2013), we have derived a more general and accurate equation for calculating the equilibrium temperature described as follows.

The calculation of equilibrium temperature is based on the energy balance equation (Eq. (3)):

$$(1 - \alpha)K^\downarrow + L^\downarrow - L^\uparrow - \lambda_v E - H = 0 \quad (3)$$

where  $\alpha$  is the water surface albedo;  $K^\downarrow$  is the downward shortwave radiation ( $\text{MJ}\cdot\text{m}^{-2}\cdot\text{d}^{-1}$ );  $L^\downarrow$  is the downward longwave radiation ( $\text{MJ}\cdot\text{m}^{-2}\cdot\text{d}^{-1}$ );  $L^\uparrow$  is the upward longwave radiation ( $\text{MJ}\cdot\text{m}^{-2}\cdot\text{d}^{-1}$ );  $\lambda_v E$  is the latent heat flux ( $\text{MJ}\cdot\text{m}^{-2}\cdot\text{d}^{-1}$ ); and  $H$  is the sensible heat flux ( $\text{MJ}\cdot\text{m}^{-2}\cdot\text{d}^{-1}$ ).

When the water temperature at the surface is within  $-30\text{ }^\circ\text{C}$  to  $50\text{ }^\circ\text{C}$ ,  $L^\downarrow$  and  $L^\uparrow$  can be approximated using Eqs. (4) and (5) (Mohseni and Stefan, 1999). Because the water body is at an equilibrium state, the outgoing longwave radiation is calculated as a function of  $T_e$ .

$$L^\downarrow = \varepsilon_a \sigma (T_a + 273.15)^4 \approx \varepsilon_a (kT_a + b) \quad (4)$$

$$L^\uparrow = \varepsilon_w \sigma (T_e + 273.15)^4 \approx \varepsilon_w (kT_e + b) \quad (5)$$

where  $\varepsilon_a$  is the emissivity of air with cloudiness factor (Satterlund, 1979; Brutsaert, 1984);  $\varepsilon_w$  is the emissivity of water (0.97 after Mohseni and Stefan, 1999);  $\sigma$  is the Stefan-Boltzman constant ( $4.9 \times 10^{-9} \text{ MJ}\cdot\text{m}^{-2}\cdot\text{K}^{-4}\cdot\text{d}^{-1}$ );  $T_a$  is the air temperature ( $^\circ\text{C}$ );  $T_e$  is the equilibrium temperature ( $^\circ\text{C}$ ); and  $k$  and  $b$  are constants of  $0.46 \text{ MJ}\cdot\text{m}^{-2}\cdot\text{d}^{-1}\cdot\text{C}^{-1}$  and  $28.38 \text{ MJ}\cdot\text{m}^{-2}\cdot\text{d}^{-1}$ , respectively.

The latent and sensible heats are calculated after Eqs. (6) and (7). As with Eq. (5),  $T_e$  is used for calculating the sensible heat flux (Eq. 7).

$$\lambda_v E = \frac{sR_n + \gamma f(u)(e_s - e_a)}{s + \gamma} = \frac{s[(1 - \alpha)K^{\downarrow} + L^{\downarrow} - L^{\uparrow}] + \gamma f(u)(e_s - e_a)}{s + \gamma} \quad (6)$$

$$H = \gamma f(u)(T_e - T_a) \quad (7)$$

After inserting Eqs. (4), (5), (6) and (7) into Eq. (3) (and some rearrangement), an equation for the equilibrium temperature (Eq. (8)) can be derived.

$$T_e = \frac{[k\varepsilon_a + f(u) \cdot (s + \gamma)] \cdot T_a + (1 - \alpha)K^{\downarrow} - b(\varepsilon_w - \varepsilon_a) - f(u)(e_s - e_a)}{k\varepsilon_w + f(u) \cdot (s + \gamma)} \quad (8)$$

Then the actual water column temperature can be estimated after de Bruin (1982) using Eqs. (9) and (10):

$$T_w = T_e + (T_{w0} - T_e) \cdot e^{-\Delta t/\tau} \quad (9)$$

$$\tau = \frac{\rho_w c_w \bar{h}}{4\sigma(T_{wb} + 273.15)^3 + f(u)(s_{wb} + \gamma)} \quad (10)$$

where  $T_w$  is the water column temperature at the current time step ( $^{\circ}\text{C}$ );  $T_{w0}$  is the water column temperature at the previous time step ( $^{\circ}\text{C}$ );  $\Delta t$  is the time step (set as one month in this study);  $\tau$  is the lag time (d);  $\rho_w$  is the water density ( $\text{kg}\cdot\text{m}^{-3}$ );  $c_w$  is the specific heat of water ( $\text{MJ}\cdot\text{kg}^{-1}\cdot\text{C}^{-1}$ );  $\bar{h}$  is the average water depth (m);  $T_{wb}$  is the wet-bulb temperature ( $^{\circ}\text{C}$ ); and  $s_{wb}$  is the slope of the saturation vapor pressure curve at  $T_{wb}$  ( $\text{kPa}\cdot\text{C}^{-1}$ ).

Various time steps for calculating equilibrium temperature have been used in previous studies (Finch and Hall, 2001; McVicar et al., 2007). Finch and Hall (2001) compared the impacts of different time steps (5, 10, and 30 days) on evaporation rate estimation and found that 30 days can still generate acceptable results. To be consistent with the TerraClimate dataset and the surface area values, we used a time step ( $\Delta t$ ) of one month here. The reservoir depth data were collected from Lehner et al. (2011). If the lake depth was  $> 20$  m, a constant value of 20 m was used. This is because the incoming radiation only affects the epilimnion layer, which is usually  $< 20$  m (Patalas, 1984). More complex reservoir stratification was not considered in this study.

The change of heat storage can subsequently be calculated after McMahon et al. (2013) by Eq. (11), which is then implemented into the Penman equation (Eq. (1)) for an improved estimation of the evaporation rate. A detailed algorithm flowchart, all the necessary equations, and a worked example are provided in the Appendix.

$$\Delta U = \rho_w c_w \bar{h} \frac{T_w - T_{w0}}{\Delta t} \quad (11)$$

### 2.3. Evaporation losses from the reservoirs

For each reservoir, the monthly evaporation volumes were calculated as the product of the monthly surface area and the monthly evaporation rate. Compared with the evaporation rate, evaporation losses from a specific reservoir are more important with regard to water management practices, as they directly affect water availability.

Using the evaporation data developed above, we introduce the reservoir evaporative losses index (RELI) for quantifying the role of evaporation in reservoir storage losses. The water storage losses of a reservoir include human water use, evaporation, and groundwater recharge. For any given reservoir, the water mass balance can be represented by Eq. (12).

$$S_t - S_{t-1} = P + Q_{in} - Q_{out} - EV - WU - \Phi \quad (12)$$

where  $S$  is the reservoir storage;  $t$  is the time step;  $P$  is the precipitation;  $Q_{in}$  and  $Q_{out}$  are the inflow and outflow of the reservoir;  $EV$  is the evaporation volume;  $WU$  is the water use of the reservoir that is directly pumped from the reservoir; and  $\Phi$  represents the other water losses.  $\Phi$  can be positive (e.g., groundwater recharge) or negative (e.g.,

groundwater discharge) (Woessner and Sullivan, 1984).

By moving the water loss components to one side and the directly measurable terms to the other side, Eq. (12) can be rearranged into Eq. (13).

$$EV + WU + \Phi = P + (Q_{in} - Q_{out}) - (S_t - S_{t-1}) \quad (13)$$

This way, the RELI can be calculated (Eq. (14)) to quantify the partitioning of evaporation in the total water losses of a given reservoir.

$$RELI = \frac{EV}{EV + WU + \Phi} = \frac{EV}{P + (Q_{in} - Q_{out}) - (S_t - S_{t-1})} \quad (14)$$

## 3. Results

### 3.1. Reservoir surface area

#### 3.1.1. Validation of reservoir surface area

Detailed validations of the GSWD and the GRSAD can be found in Pekel et al. (2016), and Zhao and Gao (2018), respectively. In addition, two reservoirs are used as examples here to demonstrate the robustness of the remotely sensed surface area results. The Amistad Reservoir is located between the USA and Mexico, and it has a maximum area of about  $150 \text{ km}^2$ . Lake Mead is located between the states of Nevada and Arizona, USA and has a maximum area of about  $600 \text{ km}^2$ . The remotely sensed surface area time series were compared with observed elevation/storage data (Fig. 3a and Fig. 4a). For the Amistad Reservoir, the coefficient of determination ( $R^2$ ) between the remotely sensed area and the observed elevation was improved from 0.38 (before the enhancement) to 0.98 (after the enhancement). For Lake Mead, the  $R^2$  was improved from 0.32 to 0.99. Since the remotely sensed area and gauge elevation/storage values are completely independent of each other, these results suggest that the area estimations can accurately capture the seasonal and inter-annual variations. For each of the two reservoirs, we also selected a high-water-level image (Fig. 3b–c, and Fig. 4b–c) and a low-water-level image (Fig. 3d–e, and Fig. 4d–e) to show the performance of the enhancement algorithm.

#### 3.1.2. Magnitude and trends of the surface area

As shown in Fig. 5a, the areas of the reservoirs have a large spatial heterogeneity ranging from  $0.1 \text{ km}^2$  to  $1350 \text{ km}^2$ . Because the surface area data from the GSWD is from Mar 1984 to Oct 2015, we selected the complete years from 1985 to 2014 to conduct all of the following trend analysis. To make the trends comparable among reservoirs, we calculated the relative trends—i.e. the value of a given trend divided by the long-term average area value (Fig. 5b). From 1985 to 2014, 429 reservoirs show insignificant trends, 134 reservoirs show negative trends, and 158 reservoirs show positive trends. The reservoirs with increasing surface area are mostly located in the eastern US while the reservoirs with decreasing surface area are located in the central and western US. Specifically, the negative trends generally have larger values than the positive trends. The average value for all of the negative trends is  $-1.0\%$  while the average value for all of the positive trends is  $0.4\%$ .

The long-term trend of surface area is generally correlated with the precipitation trend (Fig. 5b). In particular, the three central states (i.e., Texas, Oklahoma, and Louisiana) have the largest decreasing precipitation trend. As a result, the surface areas of most of the reservoirs in this region have been decreasing. In the eastern US (such as in Tennessee and North Carolina), increasing precipitation leads to a slightly increased surface area. In addition to the precipitation trend, local water management can also affect the changes of surface area. For instance, there are no significant trends for 32 of the reservoirs in Texas.

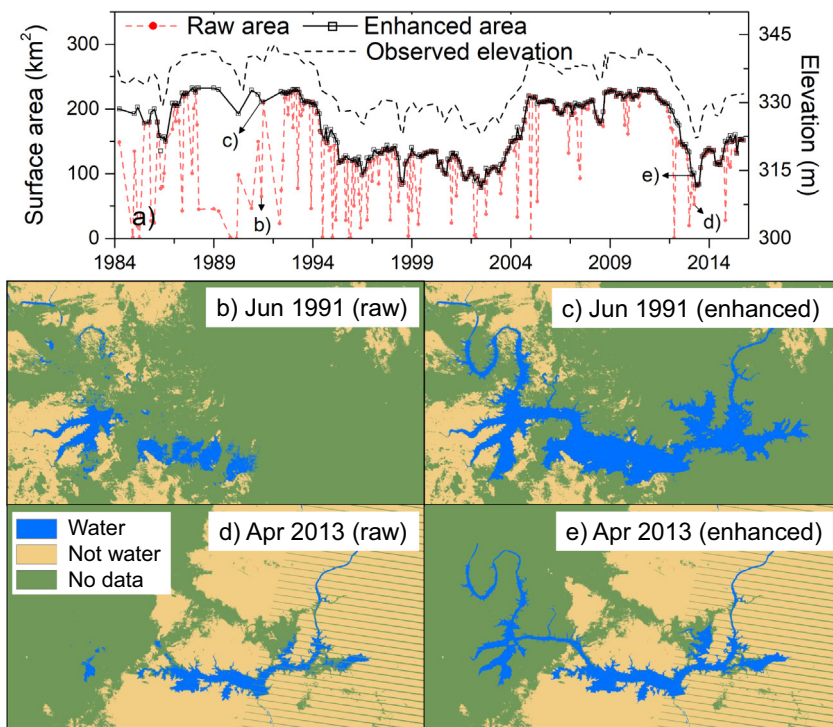


Fig. 3. Remotely sensed surface area of the Amistad Reservoir on the border between the USA and Mexico. a) Time series of reservoir surface area and gauge observed elevation from March 1984 to October 2015. b) The GSWD classification result for June 1991; c) enhanced water area from the GRSAD for June 1991; d) the GSWD classification result for April 2013; and e) enhanced water area from the GRSAD for April 2013.

### 3.2. Reservoir evaporation rate

#### 3.2.1. Validation using evaporation data collected by EC and BREB methods

As mentioned in Section 1, EC is considered to be the most reliable approach for measuring evaporation/evapotranspiration fluxes (Rimmer et al., 2009). It estimates the heat, water vapor, and carbon dioxide fluxes by directly detecting the variation of eddies at a high frequency. Uncertainties of EC open water evaporation are usually attributed to the location of the measurements, as accurate EC

measurement requires a homogeneous fetch. Both the EC instrument and the choice of processing model can also introduce uncertainties, but these should be less than those from the turbulences (Hollinger and Richardson, 2005). BREB is another widely used evaporation estimation approach that is considered to be reliable, but it is less accurate than EC (because each energy flux component can introduce errors) (Rosenberry et al., 2007). BREB approaches are typically applied to small water bodies due to the difficulties involved with quantifying the heat storage of the large ones (Friedrich et al., 2018).

Through literature review, three reservoirs with EC measurements

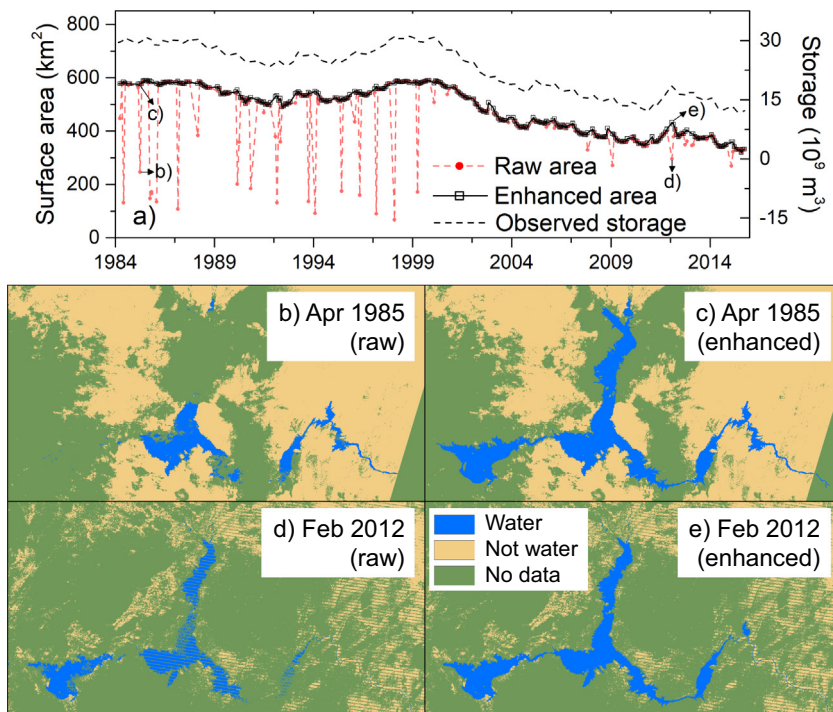
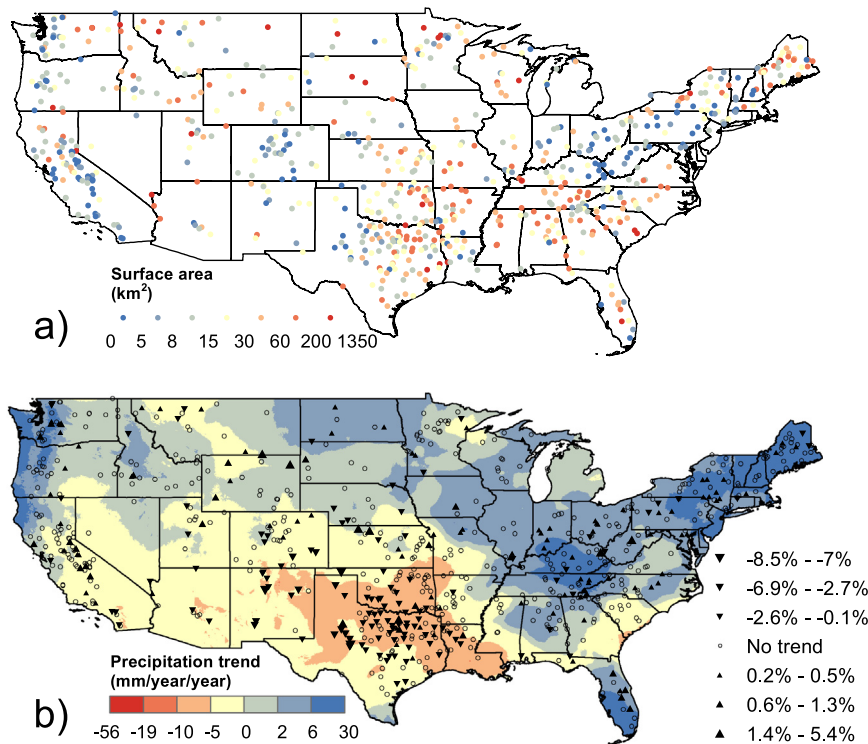
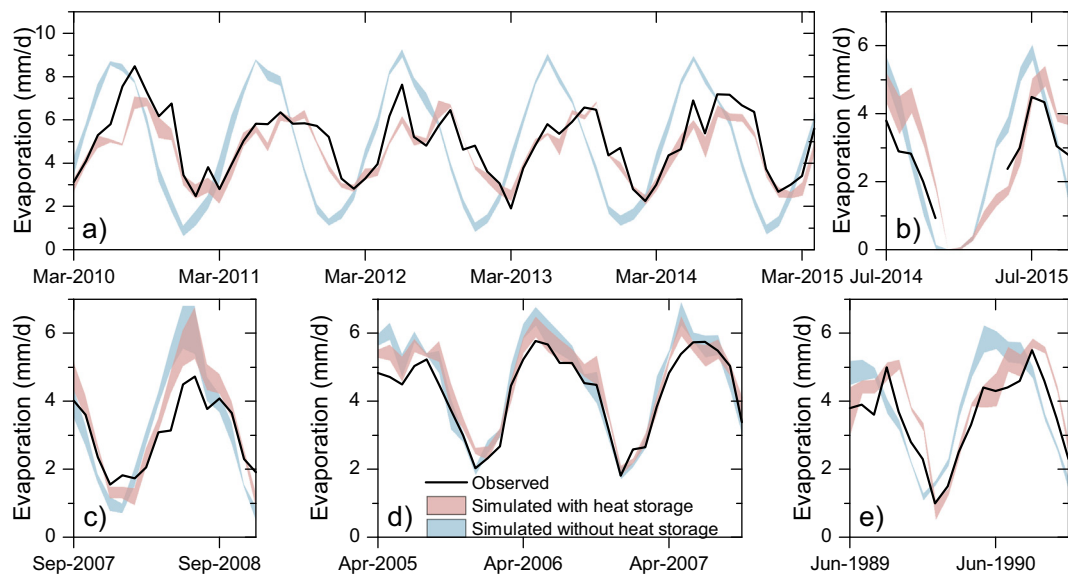


Fig. 4. Water surface extraction for Lake Mead in Nevada/Arizona. a) Time series of reservoir surface area and gauge observed storage from March 1984 to October 2015. b) The GSWD classification result for April 1985; c) enhanced water area from the GRSAD for April 1985; d) the GSWD classification result for February 2012; and e) enhanced water area from the GRSAD for February 2012.



**Fig. 5.** a) Long-term average (from 1985 to 2014) of the surface area for the 721 reservoirs and b) their trends (%/year) as detected by linear regression and Student's *t*-test with a 95% significance interval. The trends are shown as percentage values per year and were calculated by dividing the area losses per year with the long-term average areas. The precipitation trend in b) was based on TerraClimate data from 1985 to 2014.



**Fig. 6.** Comparisons of the modeled and observed evaporation rates for a) Lake Mead (Nevada/Arizona) from Mar 2010 to Dec 2011 with EC measurements; b) White Bear Lake (Minnesota) from Jul 2014 to Oct 2015 with EC measurements; c) Ross Barnett Reservoir (Mississippi) from Sep 2007 to Dec 2008 with EC measurements; d) Lake Calm (Florida) from Apr 2005 to Oct 2007 with BREB estimates; e) Lake Five-O (Florida) from Jun 1989 to Dec 1990 with BREB estimates. The shaded area represents the estimation uncertainty from different input forcing datasets (i.e., TerraClimate, NLDAS, and GLDAS).

and two reservoirs with BREB data were selected to be used as the validation sites (Fig. 6). For Lake Mead and White Bear Lake, the uncertainties from the EC estimates are 5.6% and 5.3%, respectively (Moreo, 2015; Xiao et al., 2018). The uncertainties with regard to the BREB are expected to be < 10% (Winter, 1981). The reservoir information and their error statistics are summarized in Table 1. These five lakes are located in different states with various climatic conditions. In addition, they have a wide range of depths and fetch lengths. Thus, the validation results are deemed representative.

For Lake Mead (Fig. 6a), there are clear time lags (and magnitude differences) between the observed and modeled evaporation when heat

storage is not considered. By incorporating the heat storage term into the calculation, the  $R^2$  value is improved from 0.29 to 0.84. The underestimation is likely to be caused by the advective energy (Moreo, 2015), which is not considered in our approach, and discussed further in the limitations section. White Bear Lake is the only one of these five lakes that has a decreased  $R^2$ , and yet a slightly smaller root mean square error (RMSE), after adding heat storage. This is attributed to an overestimation in 2014, as the  $R^2$  in 2015 is improved from 0.34 to 0.78. The Ross Barnett Reservoir (Fig. 6c) is a relatively shallow reservoir, which leads to small time lags. However, there is a clear overestimation of the evaporation rate in 2008 associated with NLDAS

**Table 1**  
Comparisons between the modeled and observed evaporation rates. The R<sup>2</sup> and RMSE values were calculated based on the average evaporation rate from the three input datasets.

Lake	States (latitude)	Average fetch length (km)	Depth (m)	Observation method (duration in months)	R <sup>2</sup> (with/without heat storage)	RMSE (with/without heat storage)	Relative bias (with/without heat storage)	Reference
Lake Mead	Nevada/Arizona (36.13° N)	9.76	> 20	EC (62)	0.84/0.29	0.7/2.2	−8%/−6%	Moreo, 2015
White Bear Lake	Minnesota (45.06° N)	2.53	8.3	EC (16)	0.64/0.69	0.9/1.0	21%/22%	Xiao et al., 2018
Ross Barnett Reservoir	Mississippi (32.45° N)	6.26	6	EC (16)	0.93/0.73	0.7/1.0	9%/7%	Liu et al., 2009 Liu et al., 2012
Lake Calm	Florida (28.13° N)	0.38	3	BREB (31)	0.94/0.93	0.3/0.5	7%/8%	Swancar, 2015
Lake Five-O	Florida (30.42° N)	0.27	9.5	BREB (19)	0.87/0.55	0.6/1.0	11%/10%	Sacks et al., 1994

(RMSE = 0.97 mm/d). For both TerraClimate and GLDAS, the RMSE values are 0.54 mm/d. The time lags are barely noticeable for Lake Calm (Fig. 6d), which is a 3-m deep lake in Florida. As a result of its shallow depth, the R<sup>2</sup> is only improved from 0.93 to 0.94. However, results for the deeper Lake Five-O in Florida (Fig. 6e) show clear improvement after considering heat storage.

### 3.2.2. Comparison with pan evaporation

Pan evaporation has been widely used for monitoring reservoir evaporation operationally (Tanny et al., 2008). Because of the errors introduced by multiple factors, intensive quality control processes need to be implemented with regard to the raw data to provide reliable information for further applications. Additionally, to reduce the impacts of the side heat absorption and the heat storage effect, a “pan coefficient” (i.e., the ratio of lake evaporation over pan evaporation) is usually applied to the pan observation measurements to approximate reservoir evaporation. Despite its many limitations, pan evaporation provides a source for large scale validation.

Based on the observed pan evaporation across Texas—and on the pan coefficients from NWS Technical Report 33 (TR-33)—the Texas Water Development Board (TWDB) generated a dataset containing monthly lake evaporation rates for 92 quadrangles over the entire state of Texas. The calculated evaporation rates of 86 Texas reservoirs were compared with the TWDB pan evaporation data (Fig. 7a). The R<sup>2</sup> and relative bias (in parenthesis) values between the observed pan evaporation and the simulated results of the three forcing datasets are 0.56 (−1.6%), 0.49 (3.4%), and 0.53 (−7.1%) for TerraClimate, NLDAS, and GLDAS, respectively. These relatively low R<sup>2</sup> values are caused by the fact that pan evaporation does not have a heat storage effect. By assuming a zero heat storage in the Penman Equation (Eq. (1)), the R<sup>2</sup> between the simulated evaporation rates and pan evaporation are found to be 0.82, 0.80, and 0.83, respectively for the three datasets.

Another pan evaporation dataset employed for validation is the widely used TR-33 lake evaporation, which is a climatology dataset based on long-term pan evaporation observations (with the spatially varying pan coefficients) from 1956 to 1970 in the CONUS. For each lake, we extracted the average pan evaporation rate, and then compared the value with the modeled average value from 1985 to 2014 (Fig. 7b). The R<sup>2</sup> and relative bias (in parenthesis) values between the observed pan evaporation and the simulated results of the three forcing datasets are 0.83 (−0.4%), 0.78 (5.7%), and 0.81 (−7.6%) for TerraClimate, NLDAS, and GLDAS, respectively.

### 3.2.3. Magnitude and trends of the evaporation rate

The long-term average evaporation rates are shown in Fig. 8a. Reservoirs that are located in the southern CONUS have significantly larger values than other regions due to stronger radiation. For instance, the average evaporation rate for the 86 reservoirs in Texas is 3.82 (3.53–4.09) mm/d (with the uncertainty range quoted after the average value thereafter), while the average rate for the 26 reservoirs in Minnesota is only 1.92 (1.74–2.12) mm/d.

With respect to the long-term trends of evaporation rate (Fig. 8b), most reservoirs show significant increasing trends (426 out of 721). The remaining 295 reservoirs have no significant trends (according to Student's *t*-test) and most of them are located in the northern US. The primary reason for this increase is found to be the increasing level of shortwave radiation (Fig. B-1 in the Appendix). The overall R<sup>2</sup> value between the evaporation rate trends and the shortwave radiation trends for the 721 reservoirs is 0.56. In particular, the central US shows a significant brightening trend, which leads to an increasing evaporation rate for the reservoirs in this region. The R<sup>2</sup> values between the evaporation rate trends and the trends of air temperature, vapor pressure deficit, and wind speed are 0.33, 0.53, and 0.22, respectively. In particular, the increase of vapor pressure deficit—which is caused by increased air temperature—is also highly correlated with the evaporation rate trend.

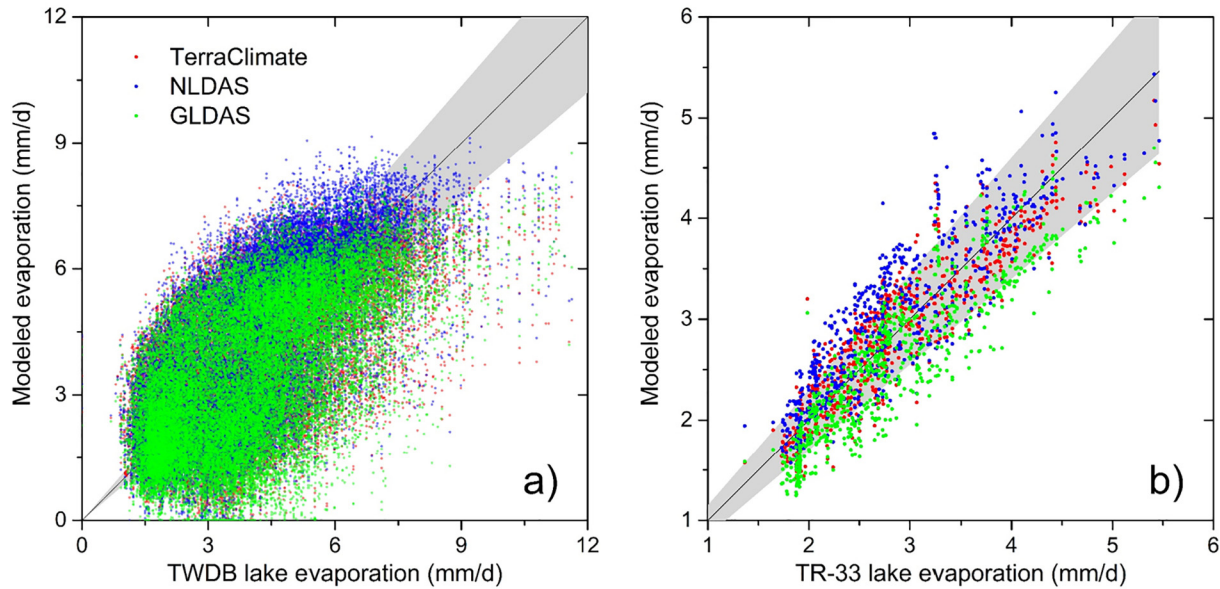


Fig. 7. Comparison between a) modeled monthly evaporation rates and TWDB scaled pan evaporation; and b) modeled long-term average evaporation rates and TR-33 scaled pan evaporation. The shaded area represents  $\pm 15\%$  of the 1:1 line.

3.3. Evaporation losses from the reservoirs

3.3.1. Magnitude and trends of evaporation volume

The volume of evaporation loss for each reservoir was estimated by multiplying the reservoir surface area by the evaporation rate (Fig. 9). For reservoirs located in the same geographical region with the same (or similar) climate, the evaporation volume is primarily determined by the surface area (see Fig. 9a as compared with Fig. 5a).

However, the evaporation volume trends for individual reservoirs can be affected by both surface area and evaporation rate trends. If

there is a significant surface area trend, the evaporation volume generally follows the same trend. For instance, the reservoirs in the states of Texas, New Mexico, Arizona, and Colorado generally show decreasing trends for both surface area and evaporation volume. However, an increasing evaporation rate trend can offset a slightly decreasing area trend for some reservoirs. Due to the severe 2010–2013 drought, 44 out of the 86 reservoirs in Texas show a decreasing surface area trend during the study period (i.e., 1985–2014), yet only 15 of them show a significant declining evaporation volume trend, while the remaining 29 show no significant trend. When there is no significant

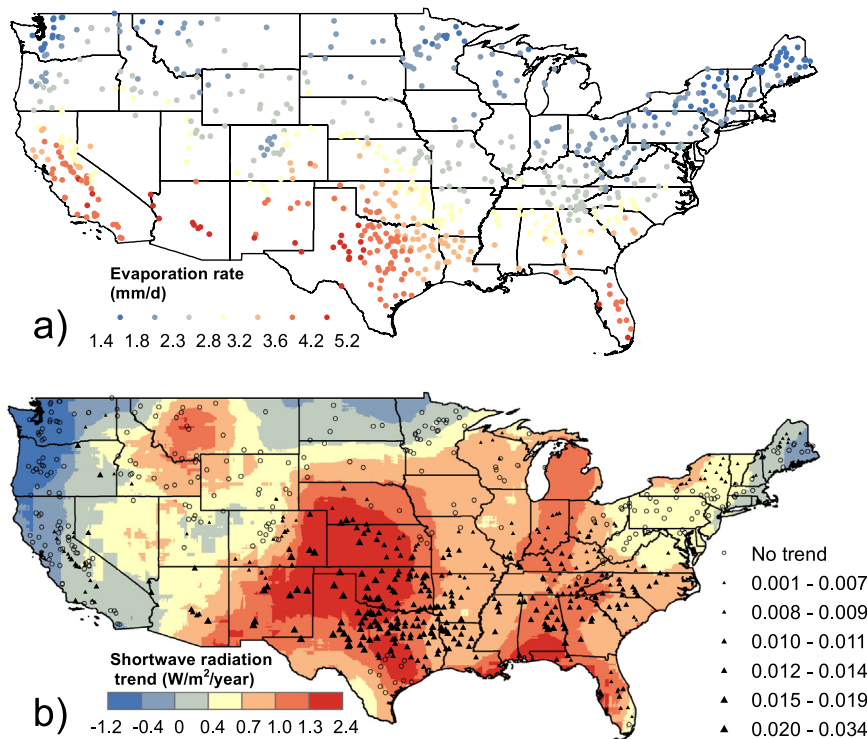
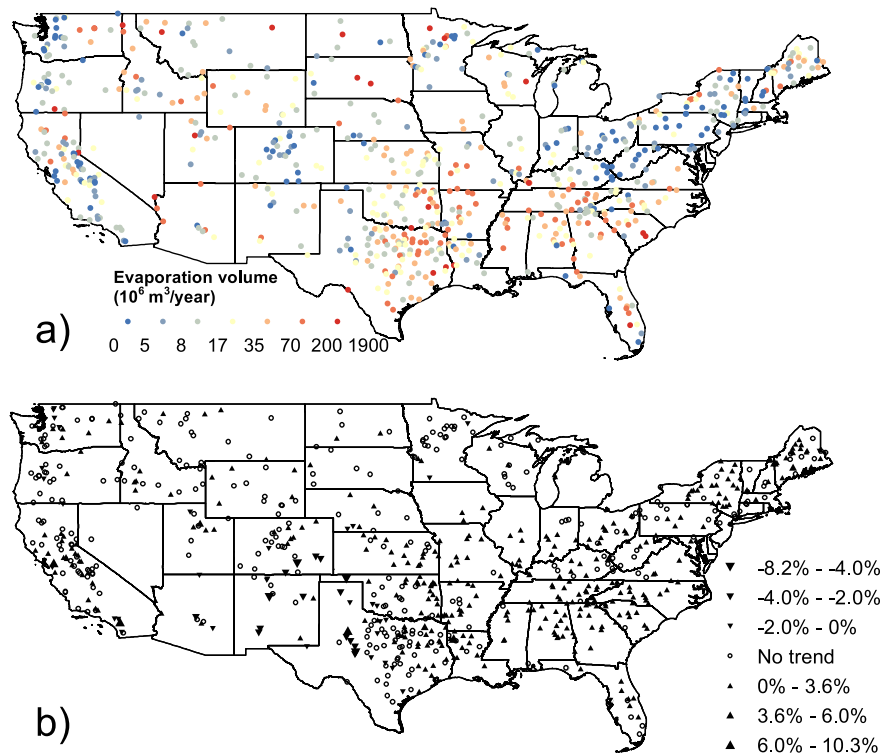


Fig. 8. a) Long-term average evaporation rates (mm/d) and b) long-term trends of evaporation rate (mm/d/year). The base map for b) shows the shortwave radiation trend from 1985 to 2014 derived from the average of TerraClimate, NLDAS, and GLDAS.



**Fig. 9.** a) Long-term average evaporation volume ( $10^6 \text{ m}^3/\text{year}$ ) and b) their trends ( $\%/ \text{year}$ ) detected by linear regression and Student's *t*-test. The trends are shown as percentage values and were calculated by dividing the annual evaporation trends with the long-term average evaporation volumes.

surface area trend, the trend in evaporation rate will propagate to the evaporation volume trend. For example, the reservoirs in the eastern US generally have increasing trends for both evaporation rate and evaporation volume. The number of reservoirs with no evaporation volume trend is 311, while those with positive and negative trends are 358 and 52, respectively.

### 3.3.2. Long term trends for the CONUS

In terms of the annual time series, the average evaporation rate, total surface area, and total evaporation volume of these 721 reservoirs have shown non-stationary characteristics (Fig. 10 and Table 2). The average evaporation rate has a significant increasing trend of about 0.0076 (0.0052–0.0106) mm/d/year ( $p = 0.00$ ). This trend is mainly caused by an increased shortwave radiation of  $0.221 \text{ W/m}^2/\text{year}$  from 1985 to 2014. These trends of shortwave radiation are consistent with the findings from Long et al. (2009) and Gan et al. (2014), which suggest that there is a global brightening trend in recent decades.

The Student's *t*-test suggests that the trend of surface area ( $-0.011 \times 10^9 \text{ m}^2/\text{year}$ ) is not statistically significant. This slightly negative trend is mostly attributed to the decreasing nature of the reservoir areas in the southwestern US (Fig. 5). The inter-annual fluctuations of the overall surface area are notable. This pattern is consistent with the wet-dry conditions in the CONUS, including the powerful El Niño event in 1997–1998 (Changnon, 2000) and the several severe flooding events in 2010 and 2011 (Vining et al., 2013).

In general, the total evaporation volume follows the evaporation rate variation, even though the surface area is also playing an important role. The maximum evaporation volume, which was caused by the high evaporation rate, occurred in 1999 with a value of  $36.83 (34.67\text{--}38.87) \times 10^9 \text{ m}^3$ . Although the evaporation rate peaked in 2012, the evaporation volume was compromised by the relatively low surface area, which was due to the severe drought that covered > 60% of the CONUS during that time period (Wolf et al., 2016). Different from the evaporation rate trends, evaporation volume trends derived from both TerraClimate and GLDAS show no notable changes while the

results from NLDAS do show significant trends. This is because the surface area has a negative trend (i.e.,  $-0.011 \times 10^9 \text{ m}^2$ ) even though it is not statistically significant according to the *t*-test. When the evaporation volume was calculated, the slight negative trend in surface area was counterbalanced by the small increasing trend in evaporation rate (in the cases of TerraClimate and GLDAS). After averaging the three datasets, the overall trend of the evaporation volume is  $0.066 \times 10^9 \text{ m}^3/\text{year}/\text{year}$ .

### 3.4. Evaporation in total water losses

Four reservoirs were selected to evaluate the role that evaporation plays in the total water losses (Fig. 11). They are Lake Mead in Nevada/Arizona, the E.V. Spence Reservoir, the Sam Rayburn Reservoir, and Wright Patman Lake in Texas. The inflow, outflow, and storage data were collected by the United States Geological Survey (USGS; <https://waterdata.usgs.gov/nwis>) (for Lake Mead) and United States Army Corps of Engineers (USACE; <http://www.swf-wc.usace.army.mil/cgi-bin/rcshtml.pl>) (for the three Texas reservoirs). The precipitation data was collected from the TerraClimate dataset.

Lake Mead—the largest reservoir in the CONUS by capacity—is critical to the regional socio-economic development (Christensen et al., 2004). Thus, the recent depletion of lake storage has raised great concern for the water managers in the Southwest (Barnett and Pierce, 2008). The average RELI value for Lake Mead from 1990 to 2014 is 65% (61%–67%). This suggests that most of the storage losses of Lake Mead are through evaporation, while the rest are attributed to the combination of direct water use (WU) (by the Las Vegas Valley) and groundwater leakage (L). The WU only accounts for the direct pumpage from the reservoir and it does not include the downstream water use. As the water level decreased, the storage losses, the evaporation, and its uncertainties all decreased (Fig. 11a).

The computed inflow (by incorporating all sources of inflow) and the observed outflow data for 29 reservoirs in Texas were provided by USACE. Following Eq. (14), the average RELI values for the E.V. Spence

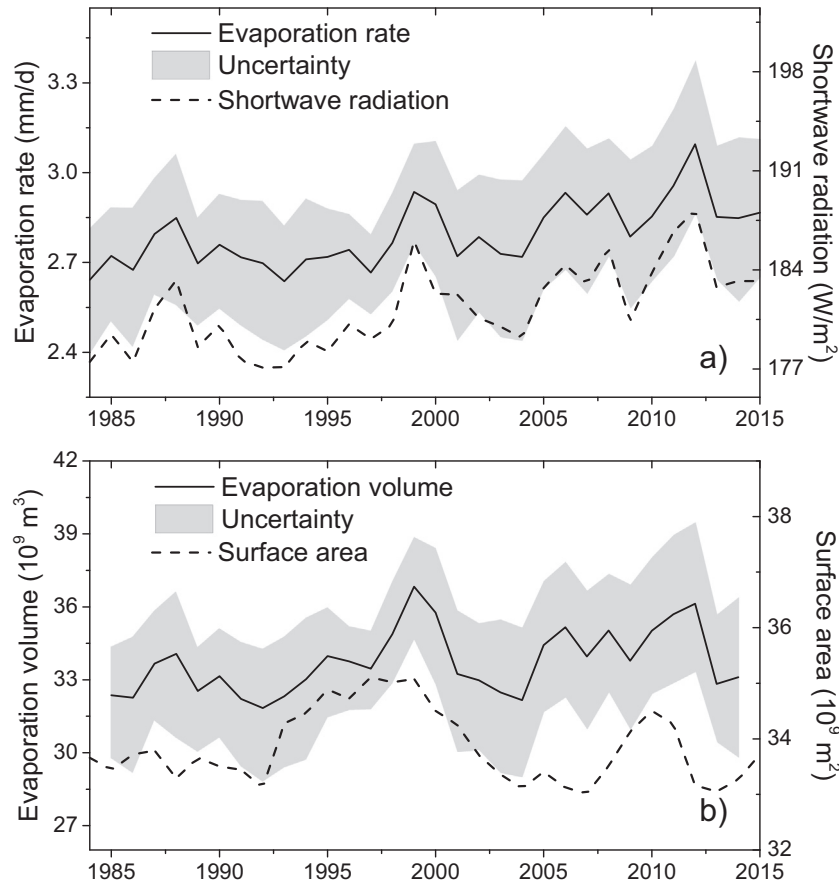


Fig. 10. Annually averaged values of a) evaporation rate and shortwave radiation, b) surface area and evaporation volume (for the 721 reservoirs). For each graph, the solid black line shows the averaged results from TerraClimate, NLDAS and GLDAS, and the shaded area represents the uncertainty.

Table 2

Student's t-test for the forcing data, evaporation rate, surface area, and evaporation volume. The first value and second value (in parentheses) in each cell represent the trend and *p*-value for the variable. The *p*-values were calculated using 95% as the confidence interval.

	TerraClimate	NLDAS	GLDAS	Average
Shortwave radiation (W/m <sup>2</sup> /year)	0.164 (0.004)	0.239 (0.000)	0.260 (0.000)	0.221 (0.000)
Air temperature (°C/year)	0.020 (0.045)	0.024 (0.021)	0.004 (0.710)	0.016 (0.104)
Vapor pressure deficit (kPa/year)	0.002 (0.088)	0.005 (0.000)	0.002 (0.072)	0.003 (0.003)
Wind speed (m/s/year)	0.001 (0.538)	0.011 (0.000)	-0.003 (0.131)	0.003 (0.033)
Evaporation rate (mm/d/year)	0.0052 (0.005)	0.0106 (0.000)	0.0069 (0.002)	0.0076 (0.000)
Surface area (10 <sup>9</sup> m <sup>2</sup> /year)		-0.011 (0.453)		
Evaporation volume (10 <sup>9</sup> m <sup>3</sup> /year/year)	0.033 (0.193)	0.105 (0.000)	0.061 (0.051)	0.066 (0.015)

Reservoir, the Sam Rayburn Reservoir, and Wright Patman Lake are 59% (55%–61%), 46% (42%–50%), and 35% (32%–38%), respectively. The shrinking of the E.V. Spence Reservoir was accompanied by reduced evaporation volume and storage losses (Fig. 11b). The RELI also decreased from 65% (in the period of 1985–1999) to 49% (in the period of 2000–2014), indicating the relatively higher loss percentage of *WU* and *L*. For the Sam Rayburn Reservoir and Wright Patman Lake (Fig. 11c and d), both evaporation volume and storage losses are

relatively stable. Located in humid eastern Texas, both reservoirs can maintain sufficient storage most of the time.

#### 4. Discussion

##### 4.1. Reservoir surface area

This long term reservoir evaporation dataset directly benefits from the high quality remotely sensed surface area estimations. Satellite images captured by VIS/NIR sensors usually suffer from multi-source contaminations including clouds, cloud shadows, and terrain shadows. For Landsat 7, the collected images also suffer from gaps due to the SLC failure. As a result, direct extraction of water area from the satellite images can lead to notable underestimations. Compared with the GSWD raw water classification results, those from the GRSAD can significantly improve the continuity of the reservoir area time series. Most of the contaminated classification results have been corrected to get the full water coverage. For example, there are 98 monthly area values (which is equivalent to > 8 years of the data record) that were corrected for the Amistad Reservoir (Fig. 3) – improving the R<sup>2</sup> between the surface area and the observed storage from 0.38 to 0.98.

The reservoir area variations are driven by a number of factors. Because reservoirs accumulate all of the water from upstream, the changes of area/storage of downstream large reservoirs can be affected by climate change at a regional scale. For instance, the surface areas of the reservoirs in the southwestern region of the US have shown significant decreasing trends, which can be explained by the reduced precipitation during the last three decades (reported in Prein et al., 2016 and Barnett and Pierce, 2008). This is particularly manifested in large reservoirs such as Lake Mead and Lake Powell. This phenomenon

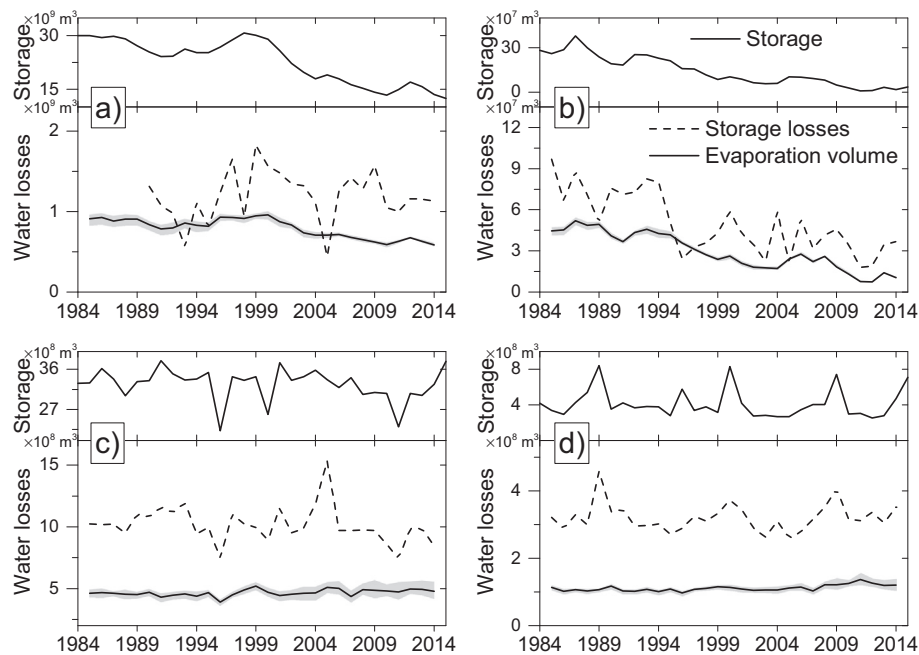


**Fig. 11.** Annual time series of the reservoir storage, storage losses (the denominator in Eq. (14)), and evaporation volume (the numerator in Eq. (14)) for a) Lake Mead in Nevada/Arizona; b) the E.V. Spence Reservoir in Texas; c) the Sam Rayburn Reservoir in Texas; and d) Wright Patman Lake in Texas.

offsets the increasing trends of reservoir surface area in other regions (Table 2). It is also worth noting that the increasing water use can be another important factor that contributes to the decreasing reservoir surface area (and thus storage), especially in areas undergoing fast urbanization (McDonald et al., 2014). For example, with the fast population growth in Texas, the surface water withdrawals for public supply increased from  $5.4 \times 10^6 \text{ m}^3$  in 1985 to  $1.26 \times 10^7 \text{ m}^3$  in 2010 (<https://water.usgs.gov/watuse>). This exacerbated the reservoir depletion during the 2010–2013 record drought (Scanlon et al., 2013).

#### 4.2. Reservoir evaporation rate

Compared to the reservoir surface area results, the evaporation rate estimates have much larger uncertainties. The errors are generally attributed to several major sources, the first of which is the meteorological forcing data. Even though TerraClimate, NLDAS, and GLDAS are all based on well-tested dataset/models, they are still not quite the same given the usage of different data sources. For example, the long-term mean shortwave radiation over these 721 reservoir is  $176.4 \text{ W/m}^2$  according to TerraClimate, but  $188.7 \text{ W/m}^2$  and  $177.8 \text{ W/m}^2$  according to NLDAS and GLDAS, respectively. Compounding these with the uncertainties from other meteorological variables, evaporation rates from TerraClimate and GLDAS turn out to be lower than those from NLDAS.

The second potential source of error is the formulation of the wind function in the Penman equation. Based on the wind functions from 19 previous studies, McJannet et al. (2012) developed a generalized wind function with the fetch effect considered. As discussed in McJannet et al. (2012), the uncertainties of the wind function include the uncertainties from the curve-fitting process, measurement errors, upwind roughness, stability conditions, and extrapolation (when applicable). Thus, the evaporation rate estimation using this generalized wind function still has large uncertainty, even though the use of a combination equation can reduce some of this by canceling the errors from the energy and aerodynamic terms (McJannet et al., 2012).

The third type of uncertainty is due to the use of some of the empirical equations. Although the Penman equation is physically based and primarily relies on four observation based meteorological variables (i.e., radiation, air temperature, vapor pressure, and wind speed), some

empirical parameterizations are involved. For example, when the wind speed is converted from 10 m (i.e., the height of the reanalysis data) to 2 m (i.e., the height used in the wind function), a logarithmic wind profile and a roughness of standard grass (0.12 m tall) are assumed (Allen et al., 1998). The roughness of open water is not used because the input for the generalized wind function is a land-based measurement. Although these assumptions can help standardize the conversion, they also introduce uncertainties (e.g. when the actual wind profile is not logarithmic, and/or the actual land cover is not grass). Another sensitive parameter is the air emissivity with the cloudiness factor ( $\epsilon_a$ ), which is used to calculate the incoming longwave radiation (Eq. (4)). As discussed in Choi et al. (2008) and Finch and Hall (2001),  $\epsilon_a$  can be affected by both the formulation of clear-sky emissivity and cloudiness.

Another potential source of error is associated with the difference between air and water surface temperature (skin temperature). The skin layer of a water body is typically  $< 1 \text{ mm}$  thick that drives the outgoing longwave radiation (Donlon et al., 2002; Talley et al., 2011). In this study, we used the air temperature as an approximation of the water skin temperature to calculate the outgoing longwave radiation component in the net radiation term (i.e.,  $R_n$  in Eq. (1)). This assumption might be challenged by the complex heat exchanges between air, skin, and beneath water (Fairall et al., 1996). However, due to the direct sensible heat fluxes between air and water surface, many studies suggested that skin temperature is more correlated with air temperature rather than bulk temperature (Trokhimovski et al., 1998; Livingstone and Lotter, 1998; Nehorai et al., 2013). Nonetheless, we acknowledge that approaches which incorporate skin temperature calculation will improve the accuracy of the evaporation rate estimates. This issue can be addressed by the incorporation of satellite derived land surface temperature (LST). Over a water body, the remotely sensed LST—such as that derived from the Moderate Resolution Imaging Spectroradiometer (MODIS) or Landsat—represents the skin temperature. However, the coarse spatial resolution of MODIS LST (1 km) and the large uncertainties of Landsat-5 LST (due to its single-channel algorithm) limit their applications in this study. Landsat-8 (launched in 2013) has two thermal bands, and the split-window algorithm can be used to significantly improve the LST accuracy and spatial resolution. Thus, future open water evaporation estimates can be improved by

incorporating Landsat-8 LST. Similarly, MODIS LST can be adopted for large lakes.

Validation results against observed (EC and BREB) evaporation rates suggest that evaporation rate estimations can be notably improved for relatively deep reservoirs (e.g., Lake Mead, White Bear Lake, and Lake Five-O) by incorporating the heat storage term into the Penman equation. Specifically, the heat storage effect delays the timing of the peak evaporation rate and reduces the seasonal variation. This phenomenon is more significant for deeper reservoirs. For large scale validation purposes, pan evaporation is the only in-situ data source. However, due to multiple factors that hamper the accuracy of monthly pan evaporation measurement, the long-term averaged evaporation validation (Fig. 7b) has a higher  $R^2$  than that of the monthly evaporation validation (Fig. 7a).

From this study we have found a significant increasing evaporation rate trend (0.0076 mm/d/year), which seemingly contradicts the declining pan evaporation. This phenomenon was reported as the “evaporation paradox” (Brutsaert and Parlange, 1998). Nonetheless, based on comprehensive assessment, several studies have concluded that the pan evaporation trend can be inversely correlated with the actual evaporation (Brutsaert, 2006; Lawrimore and Peterson, 2000; Golubev et al., 2001), which is in agreement with our results. Among the four meteorological variables, solar radiation is the primary driving force for the evaporation processes, and thus is the variable that evaporation is most sensitive to (Brutsaert, 2006; Wild, 2012; Fig. B-1). However, because our study period coincides with the global brightening period, the trend of the evaporation rate cannot be linearly extrapolated into the future (Wild, 2015). The evaporation rate is also found to be sensitive to the vapor pressure deficit, which defines the humidity gradient between the water surface and the air (McVicar et al., 2012).

The increasing air temperature can enhance the evaporation process by increasing the Bowen ratio, with less sensible heat but more latent heat (Wang et al., 2018). Our results (Fig. B-1b) also show a correlation between evaporation rate changes and air temperature trends. With respect to the wind speed, none of the three reanalysis based forcing datasets have shown a significant stilling trend across the entire CONUS—a phenomenon suggested by other studies (McVicar et al., 2012; Vautard et al., 2010). This is because the reanalysis used the rawinsonde data, which are upper-air measurements instead of earth surface observations. In addition, the global stilling is still unexplained. It can be caused by a variety of factors including increased ground roughness (although this possibly does not apply on open water surface), global circulation, and even possibly a worn bearing in the anemometer used for measurement (Azorin-Molina et al., 2018).

Although there are a number of studies suggesting an increasing trend for evapotranspiration over the CONUS (0.95 mm/year/year for 1950–2000 in Walter et al., 2004; 0.32 mm/year/year for 2000–2014 in Mu et al., 2011), there have been no findings about reservoir evaporation losses and trends across the entire the region. Nonetheless, increased lake evaporation has been reported in several other sub-continental regions, such as the Canadian Prairies (Burn and Hesch, 2007) and subtropical China (Hu et al., 2017). In addition, the future lake evaporation rate has been projected to increase in several studies (Australia lakes in Johnson and Sharma, 2010; Great Lakes in Lofgren et al., 2002; southeastern Australia reservoirs in McGloin et al., 2016; global lakes in Wang et al., 2018). In contrast, lake evaporation in the Tibetan Plateau has shown a decreasing trend, owing to the reduced wind speed and the shortened duration of solar radiation (Lei et al., 2014; Ma et al., 2016). Because of the inter-regional diversity, thorough investigations of the sensitivities to the trends of the meteorological forcings are necessary to identify the reasons for the evaporation changes (McVicar et al., 2012).

To quantify the regional reservoir evaporation, an alternative modeling method that is widely used is the Complementary Relationship Lake Evaporation method (CRLE; Morton, 1983; Morton, 1994; Huntington and McEvoy, 2011; Huntington et al., 2015), which is

based on the Bouchet hypothesis (Bouchet, 1963). A brief comparison between CRLE estimates from Huntington et al. (2015) as well as other studies (shown in the Appendix) and estimates using our approach had an  $R^2$ , RMSE, and RB of 0.86, 0.35 mm/d, and  $-4.3\%$ , respectively across 16 reservoirs in the U.S.. The CRLE method is also capable of simulating the heat storage changes, but it does not use the wind speed term in the calculation of the evaporation. According to Morton (1994), the vapor transfer coefficient in the evaporation equation is independent of wind speed because 1) surface roughness is more dominant than wind speed in effective vapor transfer; 2) atmospheric instability increases the process of vapor transfer, especially at low wind speeds; and 3) wind speed measurements have large uncertainties. Thus, Morton assumed that the incorporation of wind speed might increase the uncertainty of evaporation rather than reducing it. Yet, there are also some limitations with regard to CRLE: 1) it is still to be determined whether the complementary relationship is indeed asymmetric (Szilagyi and Jozsa, 2008; McMahon et al., 2013); and 2) the fetch effect, which relies on the size of the open water surface, is generalized (Morton, 1986).

#### 4.3. Evaporation losses from the reservoirs

The total evaporation from the 721 reservoirs is one of the major contributors to the storage losses. The average evaporation volume is  $33.73 (31.00\text{--}36.24) \times 10^9 \text{ m}^3$  per year from 1985 to 2014, which is equivalent to 93% (85–100%) of the surface water that was used for public supply in the United States in 2010 ( $36.34 \times 10^9 \text{ m}^3$  according to Maupin et al., 2014). Specifically, the reservoirs that are located in the arid southwestern US suggest that evaporation accounts for a large portion of the overall storage losses. For example, the RELI for Lake Mead (Arizona and Nevada) is 65% and the RELI for E.V. Spence reservoir (Texas) is 59%, both contributing significantly to the long-term reservoir depletion.

Although the evaporation rates show an increasing trend for all three datasets, the evaporation volume trends contain substantial uncertainties. Both TerraClimate and GLDAS show no significant trend for the total evaporation volume. This is because the decreasing (even not statistically significant) trend of surface area counterbalances the slight increasing trend of evaporation rate. Specifically, the reservoirs with decreasing surface area trends are mostly located in the southwestern US, where they are subjected to the most intensive evaporation processes. Thus, even though the total number of these reservoirs is small, their combined contribution to the total evaporation volume is notable. For NLDAS, the results suggest a significant evaporation volume trend, which is caused by the more quickly increasing evaporation rate than that from TerraClimate and GLDAS.

#### 4.4. Potential applications

A relevant study based on MODIS data found that global open water evaporation accounts for 58% of the terrestrial secondary evaporation (i.e., evaporation from all inland water bodies, including irrigated area; van Dijk et al., 2018). However, due to the challenges involved with estimating reservoir area and evaporation rate, there have been very few studies focused on reporting evaporation over individual reservoirs at a large scale. Most studies have either focused on a single reservoir or a catchment scale such that the wind function can be calibrated (Gianniu and Antonopoulos, 2007; Valiantzas, 2006; Linacre, 1993). On a large scale, the evaporation rate is generally reported separately without considering the surface area changes (Alvarez et al., 2008; Mekonnen et al., 2015). By considering the heat storage term and adopting a generalized wind function, this study has improved upon the Penman equation which allows for estimating the evaporation rate more accurately. Furthermore, the surface area data were extracted from a remotely sensed dataset for which an enhancement algorithm was applied to repair image contaminations. Subsequently, monthly

time series of evaporation for the 721 reservoirs in the CONUS over a long-term were generated.

This evaporation dataset can help decision makers better manage water use for different purposes. First, the evaporation dataset from this study can support the allocation of water rights. For example, in the State of Texas, water rights are allocated to each water user for legal extraction of surface water. Yet reservoir evaporation in the current water rights allocation system has been represented in a simple manner. As a result, water resources could be excessively exploited or not sufficiently used. Second, in addition to evaporation, another major source of reservoir water loss is leakage to groundwater—which is extremely difficult to quantify due to the complex physical processes involved. By employing the evaporation volume from this dataset in the reservoir water balance equation, reservoir leakage can be derived (when inflow and outflow data are also available). The results can potentially improve the water management efficiency for both surface water and groundwater. Third, it can be used for quantifying the blue water footprint from hydropower generation. By constructing a reservoir, the original evapotranspiration within the impounding area would be replaced by open water evaporation, which might be significantly larger. This is especially true in the western US (Mekonnen and Hoekstra, 2012). Therefore, quantification of the blue water footprint is important for future energy policies. Last, this data product potentially can be used for improving reservoir operation rules under a changing climate. For instance, reservoir managers might need to increase the conservation pool level (whose water is used for water supply) in order to counterbalance the enhanced evaporation of some reservoirs.

This algorithm can be potentially used for near real-time applications. Benefiting from the recent launches of several earth observation satellites (e.g., USGS Landsat-8, European Space Agency Sentinel-2, and Chinese Gaofen program), high resolution optical imageries have become more frequently available. By applying image classification and enhancement algorithms on cloud computing platforms such as the Google Earth Engine (Gorelick et al., 2017), submonthly or even daily near real-time reservoir surface area can be estimated. Then evaporation volumes can be obtained by combining these area values with evaporation rates derived from the updated climate forcing dataset.

#### 4.5. Algorithm caveats

Although the algorithms developed in this study focus on estimating evaporation accurately by addressing many of the constraints that were identified in previous studies, there are still several limitations that are worth noting. First, because there are barely any observations directly collected over lakes, the evaporation rate errors associated with the forcing data (e.g., wind speed, shortwave/longwave radiation) are difficult to quantify. Thus, the uncertainties from the forcing data were approximated using the spread from three reanalysis datasets. Second, due to the lack of reservoir bathymetry information at a large scale, the effects of stratification on the water column temperature were not considered. Third, the advective heat fluxes transferred by inflow, outflow, and groundwater are not included. Varying by reservoir, the advective heat flux can be a significant energy source for evaporation (Friedrich et al., 2018). For example, some reservoirs release water at the dam intake depth, at which the water has a notably different temperature from that at the surface. In these cases, the evaporation rate might be underestimated in the summer months and overestimated in the winter months. Another simplification of the algorithm is associated with ice coverage on the reservoirs. When the calculated water temperature—or the evaporation rate—is less than zero, the evaporation rate is set as zero. For more accurate results, the ice cover percentage can be calculated through the original Landsat image classification or the quality control band. Then the evaporation rate can be adjusted accordingly.

## 5. Conclusion

This study presents an advanced algorithm framework for reservoir evaporation quantification at a large scale. By applying the algorithm to 721 reservoirs in the CONUS, a first of its kind continentally consistent and locally practical evaporation data product was generated, providing significant benefits to the water resources management, hydrology, and remote sensing communities. The major conclusions are as follows:

1. For the 721 reservoirs in the CONUS, long term average evaporation was found to be  $33.73 (31.00\text{--}36.24) \times 10^9 \text{ m}^3$  per year from 1985 to 2014. This amount is equivalent to 93% (85–100%) of the surface water used for public supply in the United States in 2010.
2. Due to the increasing trend of shortwave radiation, the evaporation rate has been elevated accordingly ( $0.0076 \text{ mm/d/year}$ ). The long-term trends of reservoir surface areas are largely connected with regional climate and local water management practices.
3. The evaporation volume trend for individual reservoirs can be affected by both surface area trend (mostly in the southwestern US) and the evaporation rate trend (mostly in the eastern US). For all of the 721 reservoirs, different meteorological datasets show various trends (i.e., insignificant trends for TerraClimate and GLDAS while significant trends for NLDAS). On average, the increasing trend for the evaporation volume is  $0.066 \times 10^9 \text{ m}^3$  per year from 1985 to 2014.
4. Although there are some limitations with the algorithm (e.g. the robustness needs to be further tested), this dataset has shown its potential to support many applications directed toward more sustainable water resources management in a changing environment.

## Acknowledgement

The dataset containing the evaporation time series of the 721 reservoirs will be publicly available online at <https://ceprofs.civil.tamu.edu/hgao/> and at <https://dataverse.tdl.org/dataverse/tamu>.

This research was supported by the NASA Science of Terra, Aqua, and Suomi NPP (TASNPP) Program (80NSSC18K0939), and the Earth and Space Science Fellowship (NESSF) Program (80NSSC17K0358). It was also partially supported by the U.S. Department of Energy Water Power Technologies Office as a part of the SECURE Water Act Section 9505 Assessment. It has benefitted from the usage of the Google Earth Engine platform and the Texas A&M Supercomputing Facility. The lake evaporation data for Texas reservoirs were collected from the Texas Water Development Board. We would also like to thank Dr. Tim R. McVicar (the Associate Editor), Dr. Albert van Dijk, Dr. Justin Huntington, and another anonymous reviewers for the detailed suggestions toward helping to improve the manuscript.

## Appendix A. Supplementary data

Supplementary data to this article can be found online at <https://doi.org/10.1016/j.rse.2019.03.015>.

## References

- Abatzoglou, J.T., Dobrowski, S.Z., Parks, S.A., Hegewisch, K.C., 2018. TerraClimate, a high-resolution global dataset of monthly climate and climatic water balance from 1958–2015. *Scientific Data* 5, 170191.
- Abtew, W., 2001. Evaporation estimation for Lake Okeechobee in south Florida. *J. Irrig. Drain. Eng.* 127 (3), 140–147.
- Ali, S., Ghosh, N.C., Singh, R., 2008. Evaluating best evaporation estimate model for water surface evaporation in semi-arid region, India. *Hydrol. Process.* 22 (8), 1093–1106.
- Allen, R.G., Pereira, L.S., Raes, D., Smith, M., 1998. Crop evapotranspiration-guidelines for computing crop water requirements-FAO irrigation and drainage paper 56, FAO. Rome 300 (9), D05109.
- Alvarez, V.M., González-Real, M., Baille, A., Valero, J.M., Elvira, B.G., 2008. Regional

- assessment of evaporation from agricultural irrigation reservoirs in a semiarid climate. *Agric. Water Manag.* 95 (9), 1056–1066.
- Assouline, S., Li, D., Tyler, S., Tanny, J., Cohen, S., Bou-Zeid, E., Parlange, M., Katul, G.G., 2016. On the variability of the Priestley-Taylor coefficient over water bodies. *Water Resour. Res.* 52 (1), 150–163.
- Azorin-Molina, C., Asin, J., McVicar, T.R., Minola, L., Lopez-Moreno, J.I., Vicente-Serrano, S.M., Chen, D., 2018. Evaluating anemometer drift: a statistical approach to correct biases in wind speed measurement. *Atmos. Res.* 203, 175–188.
- Barnett, T.P., Pierce, D.W., 2008. When will Lake Mead go dry? *Water Resour. Res.* 44 (3).
- Bogan, T., Mohseni, O., Stefan, H.G., 2003. Stream temperature-equilibrium temperature relationship. *Water Resour. Res.* 39 (9).
- Bouchet, R.J., 1963. Evapotranspiration réelle et potentielle, signification climatique. *IAHS Publ.* 62, 134–142.
- Brutsaert, W., 1984. *Evaporation into the Atmosphere: Theory, History and Applications*. (Springer Science & Business Media).
- Brutsaert, W., 2006. Indications of increasing land surface evaporation during the second half of the 20th century. *Geophys. Res. Lett.* 33 (20).
- Brutsaert, W., Parlange, M., 1998. Hydrologic cycle explains the evaporation paradox. *Nature* 396 (6706), 30.
- Burn, D.H., Hesch, N.M., 2007. Trends in evaporation for the Canadian prairies. *J. Hydrol.* 336 (1), 61–73.
- Busker, T., de Roo, A., Gelati, E., Schwatke, C., Adamovic, M., Bisselink, B., Pekel, J.F., Cottam, A., 2018. A global lake and reservoir volume analysis using a surface water dataset and satellite altimetry. *Hydrol. Earth Syst. Sci. Discuss.* 2018, 1–32.
- Caissie, D., Satish, M.G., El-Jabi, N., 2005. Predicting river water temperatures using the equilibrium temperature concept with application on Miramichi River catchments (New Brunswick, Canada). *Hydrol. Process.* 19 (11), 2137–2159.
- Changnon, S.A., 2000. *El Niño 1997–1998: The Climate Event of the Century*. Oxford University Press.
- Chao, B.F., Wu, Y., Li, Y., 2008. Impact of artificial reservoir water impoundment on global sea level. *Science* 320 (5873), 212–214.
- Choi, M., Jacobs, J.M., Kustas, W.P., 2008. Assessment of clear and cloudy sky parameterizations for daily downwelling longwave radiation over different land surfaces in Florida, USA. *Geophys. Res. Lett.* 35 (20).
- Christensen, N.S., Wood, A.W., Voinis, N., Lettenmaier, D.P., Palmer, R.N., 2004. The effects of climate change on the hydrology and water resources of the Colorado River Basin. *Clim. Chang.* 62 (1), 337–363.
- de Bruin, H., 1982. Temperature and energy balance of a water reservoir determined from standard weather data of a land station. *J. Hydrol.* 59 (3–4), 261–274.
- Donchyts, G., Baart, F., Winsemius, H., Gorelick, N., Kwadijk, J., van de Giesen, N., 2016. Earth's surface water change over the past 30 years. *Nat. Clim. Chang.* 6 (9), 810–813.
- Donlon, C.J., Minnett, P.J., Gentemann, C., Nightingale, T.J., Barton, I.J., Ward, B., Murray, M.J., 2002. Toward improved validation of satellite sea surface skin temperature measurements for climate research. *J. Clim.* 15 (4), 353–369.
- dos Reis, R.J., Dias, N.L.S., 1998. Multi-season lake evaporation: energy-budget estimates and CRLE model assessment with limited meteorological observations. *J. Hydrol.* 208 (3), 135–147.
- Edinger, J.E., Duttweiler, D.W., Geyer, J.C., 1968. The response of water temperatures to meteorological conditions. *Water Resour. Res.* 4 (5), 1137–1143.
- Eichinger, W.E., Parlange, M.B., Stricker, H., 1996. On the concept of equilibrium evaporation and the value of the Priestley-Taylor coefficient. *Water Resour. Res.* 32 (1), 161–164.
- Fairall, C.W., Bradley, E.F., Rogers, D.P., Edson, J.B., Young, G.S., 1996. Bulk parameterization of air-sea fluxes for tropical ocean-global atmosphere coupled-ocean atmosphere response experiment. *Journal of Geophysical Research: Oceans* 101 (C2), 3747–3764.
- Finch, J.W., 2001. A comparison between measured and modelled open water evaporation from a reservoir in south-East England. *Hydrol. Process.* 15 (14), 2771–2778.
- Finch, J., Hall, R., 2001. *Estimation of Open Water Evaporation: A Review of Methods*. Agency, Environment.
- Flint, A.L., Childs, S.W., 1991. Use of the Priestley-Taylor evaporation equation for soil water limited conditions in a small forest clearcut. *Agric. For. Meteorol.* 56 (3–4), 247–260.
- Friedrich, K., Grossman, R.L., Huntington, J., Blanken, P.D., Lenters, J., Holman, K.D., Gochis, D., Livneh, B., Prairie, J., Skeie, E., 2018. Reservoir evaporation in the Western United States: current science, challenges, and future needs. *Bull. Am. Meteorol. Soc.* 99 (1), 167–187.
- Gan, C.-M., Pleim, J., Mathur, R., Hogrefe, C., Long, C.N., Xing, J., Roselle, S., Wei, C., 2014. Assessment of the effect of air pollution controls on trends in shortwave radiation over the United States from 1995 through 2010 from multiple observation networks. *Atmos. Chem. Phys.* 14 (3), 1701–1715.
- Gao, H., 2015. *Satellite remote sensing of large lakes and reservoirs: from elevation and area to storage*. Wiley Interdiscip. Rev. Water 2 (2), 147–157.
- Gianniou, S.K., Antonopoulos, V.Z., 2007. Evaporation and energy budget in Lake Vegoritis, Greece. *J. Hydrol.* 345 (3–4), 212–223.
- Golubev, V.S., Lawrimore, J.H., Groisman, P.Y., Speranskaya, N.A., Zhuravin, S.A., Menne, M.J., Peterson, T.C., Malone, R.W., 2001. Evaporation changes over the contiguous United States and the former USSR: a reassessment. *Geophys. Res. Lett.* 28 (13), 2665–2668.
- Gorelick, N., Hancher, M., Dixon, M., Ilyushchenko, S., Thau, D., Moore, R., 2017. Google earth engine: planetary-scale geospatial analysis for everyone. *Remote Sens. Environ.* 202, 18–27.
- Graf, W.L., 1999. Dam nation: a geographic census of American dams and their large-scale hydrologic impacts. *Water Resour. Res.* 35 (4), 1305–1311.
- Harwell, G.R., 2012. *Estimation of Evaporation from Open Water—A Review of Selected Studies*, Summary of US Army Corps of Engineers Data Collection and Methods, and Evaluation of Two Methods for Estimation of Evaporation from Five Reservoirs in Texas, Rep 2328-0328. (US Geological Survey).
- Hollinger, D., Richardson, A., 2005. Uncertainty in eddy covariance measurements and its application to physiological models. *Tree Physiol.* 25 (7), 873–885.
- Hu, C., Wang, Y., Wang, W., Liu, S., Piao, M., Xiao, W., Lee, X., 2017. Trends in evaporation of a large subtropical lake. *Theor. Appl. Climatol.* 129 (1–2), 159–170.
- Huntington, J.L., McEvoy, D., 2011. *Climatological estimates of open water evaporation from selected Truckee and Carson River basin water bodies, California and Nevada*, Desert Research Institute. Publication No. 41254 (35p).
- Huntington, J., Gangopadhyay, S., Spears, M., Allen, R., King, D., Morton, C., Harrison, A., McEvoy, D., Joros, A., Pruitt, T., 2015. West-wide climate risk assessments: Irrigation demand and reservoir evaporation projections. In: US Bureau of Reclamation (Ed.), Technical memorandum No. 68-68210-2014-01, (196p).
- Johnson, F., Sharma, A., 2010. A comparison of Australian open water body evaporation trends for current and future climates estimated from Class A evaporation pans and general circulation models. *J. Hydrometeorol.* 11 (1), 105–121.
- Khandelwal, A., Karpatne, A., Marlier, M.E., Kim, J., Lettenmaier, D.P., Kumar, V., 2017. An approach for global monitoring of surface water extent variations in reservoirs using MODIS data. *Remote Sens. Environ.* 202, 113–128.
- Lawrimore, J.H., Peterson, T.C., 2000. Pan evaporation trends in dry and humid regions of the United States. *J. Hydrometeorol.* 1 (6), 543–546.
- Lehner, B., Liermann, C.R., Revenga, C., Vörösmarty, C., Fekete, B., Crouzet, P., Döll, P., Endejan, M., Frenken, K., Magome, J., Nilsson, C., 2011. High-resolution mapping of the world's reservoirs and dams for sustainable river-flow management. *Front. Ecol. Environ.* 9 (9), 494–502.
- Lei, Y., Yang, K., Wang, B., Sheng, Y., Bird, B.W., Zhang, G., Tian, L., 2014. Response of inland lake dynamics over the Tibetan Plateau to climate change. *Clim. Chang.* 125 (2), 281–290.
- Linacre, E.T., 1993. Data-sparse estimation of lake evaporation, using a simplified Penman equation. *Agric. For. Meteorol.* 64 (3), 237–256.
- Liu, H., Zhang, Y., Liu, S., Jiang, H., Sheng, L., Williams, Q.L., 2009. Eddy covariance measurements of surface energy budget and evaporation in a cool season over southern open water in Mississippi. *Journal of Geophysical Research: Atmospheres* 114 (D4).
- Liu, H., Zhang, Q., Dowler, G., 2012. Environmental controls on the surface energy budget over a large southern inland water in the United States: an analysis of one-year eddy covariance flux data. *J. Hydrometeorol.* 13 (6), 1893–1910.
- Livingstone, D.M., Lotter, A.F., 1998. The relationship between air and water temperatures in lakes of the Swiss Plateau: a case study with paleolimnological implications. *J. Paleolimnol.* 19 (2), 181–198.
- Lofgren, B.M., Quinn, F.H., Clites, A.H., Assel, R.A., Eberhardt, A.J., Luukkonen, C.L., 2002. Evaluation of potential impacts on Great Lakes water resources based on climate scenarios of two GCMs. *J. Great Lakes Res.* 28 (4), 537–554.
- Long, C.N., Dutton, E.G., Augustine, J., Wiscombe, W., Wild, M., McFarlane, S.A., Flynn, C.J., 2009. Significant decadal brightening of downwelling shortwave in the continental United States. *Journal of Geophysical Research: Atmospheres* 114 (D10).
- Luo, L., Robock, A., Mitchell, K.E., Houser, P.R., Wood, E.F., Schaake, J.C., Lohmann, D., Cosgrove, B., Wen, F., Sheffield, J., 2003. Validation of the North American land data assimilation system (NLDAS) retrospective forcing over the southern Great Plains. *Journal of Geophysical Research: Atmospheres* 108 (D22).
- Ma, N., Szilagyi, J., Niu, G.-Y., Zhang, Y., Zhang, T., Wang, B., Wu, Y., 2016. Evaporation variability of Nam Co Lake in the Tibetan Plateau and its role in recent rapid lake expansion. *J. Hydrol.* 537, 27–35.
- Maupin, M.A., Kenny, J.F., Hutson, S.S., Lovelace, J.K., Barber, N.L., Linsey, K.S., 2014. *Estimated Use of Water in the United States in 2010*, Rep 2330-5703. Survey, US Geological.
- McDonald, R.I., Weber, K., Padowski, J., Flörke, M., Schneider, C., Green, P.A., Gleeson, T., Eckman, S., Lehner, B., Balk, D., 2014. Water on an urban planet: urbanization and the reach of urban water infrastructure. *Glob. Environ. Chang.* 27, 96–105.
- McFeeters, S.K., 1996. The use of the Normalized Difference Water Index (NDWI) in the delineation of open water features. *Int. J. Remote Sens.* 17 (7), 1425–1432.
- McGloin, R., McGowan, H., McJannet, D., 2016. The potential effects of anthropogenic climate change on evaporation from water storage reservoirs within the Lockyer Catchment, south-east Queensland, Australia. *Mar. Freshw. Res.* 67 (10), 1512–1521.
- McJannet, D., Webster, I., Stenson, M., Sherman, B., 2008. *Estimating Open Water Evaporation for the Murray Darling Basin*. Report for CSIRO, Australia.
- McJannet, D.L., Webster, I.T., Cook, F.J., 2012. An area-dependent wind function for estimating open water evaporation using land-based meteorological data. *Environ. Model. Softw.* 31, 76–83.
- McJannet, D., Hawdon, A., Van Niel, T., Boadle, D., Baker, B., Trefry, M., Rea, I., 2017. Measurements of evaporation from a mine void lake and testing of modelling approaches. *J. Hydrol.* 555, 631–647.
- McMahon, T., Peel, M., Lowe, L., Srikanthan, R., McVicar, T., 2013. Estimating actual, potential, reference crop and pan evaporation using standard meteorological data: a pragmatic synthesis. *Hydrol. Earth Syst. Sci.* 17 (4), 1331.
- McVicar, T.R., Li, L., Van Niel, T.G., Zhang, L., Li, R., Yang, Q., Zhang, X., Mu, X., Wen, Z., Liu, W., 2007. Developing a decision support tool for China's re-vegetation program: simulating regional impacts of afforestation on average annual streamflow in the Loess Plateau. *For. Ecol. Manag.* 251 (1–2), 65–81.
- McVicar, T.R., et al., 2012. Global review and synthesis of trends in observed terrestrial near-surface wind speeds: implications for evaporation. *J. Hydrol.* 416–417, 182–205.
- Mekonnen, M., Hoekstra, A., 2012. The blue water footprint of electricity from hydro-power. *Hydrol. Earth Syst. Sci.* 16, 179–187.
- Mekonnen, M.M., Gerbens-Leenes, P., Hoekstra, A.Y., 2015. The consumptive water footprint of electricity and heat: a global assessment. *Environmental Science: Water*

- Research & Technology 1 (3), 285–297.
- Moene, A.F., Hartogensis, O.K., Beyrich, F., 2009. Developments in scintillometry. *Bull. Am. Meteorol. Soc.* 90 (5), 694–698.
- Mohseni, O., Stefan, H., 1999. Stream temperature/air temperature relationship: a physical interpretation. *J. Hydrol.* 218 (3), 128–141.
- Monteith, J.L., 1965. *Evaporation and Environment*, Paper Presented at Symp. Soc. Exp. Biol.
- Moreo, M.T., 2015. *Evaporation Data from Lake Mead and Lake Mohave, Nevada and Arizona, March 2010 through April 2015: U.S. Geological Survey Data Release. US Geological Survey* <https://doi.org/10.5066/F79C6VG3>. Rep. 2328-0328.
- Morton, F., 1979. Climatological estimates of lake evaporation. *Water Resour. Res.* 15 (1), 64–76.
- Morton, F.I., 1983. Operational estimates of areal evapotranspiration and their significance to the science and practice of hydrology. *J. Hydrol.* 66 (1–4), 1–76.
- Morton, F.I., 1986. Practical estimates of lake evaporation. *J. Clim. Appl. Meteorol.* 25 (3), 371–387.
- Morton, F., 1994. Evaporation research—a critical review and its lessons for the environmental sciences. *Crit. Rev. Environ. Sci. Technol.* 24 (3), 237–280.
- Mu, Q., Zhao, M., Running, S.W., 2011. Improvements to a MODIS global terrestrial evapotranspiration algorithm. *Remote Sens. Environ.* 115 (8), 1781–1800.
- Nehorai, R., Lensky, N., Brenner, S., Lensky, I., 2013. The dynamics of the skin temperature of the Dead Sea. *Adv. Meteorol.* 2013.
- Ohmura, A., Wild, M., 2002. Is the hydrological cycle accelerating? *Science* 298 (5597), 1345–1346.
- Organisation for Economic Co-operation and Development, 2008. *OECD environmental outlook to 2030. Organisation for Economic Co-operation and Development*. 517.
- Patalas, K., 1984. Mid-summer mixing depths of lakes of different latitudes. *Verhandlung Internationale Vereinigung Limnologie* 22 (1).
- Pekel, J.-F., Cottam, A., Gorelick, N., Belward, A.S., 2016. High-resolution mapping of global surface water and its long-term changes. *Nature* 540 (7633), 418–422.
- Penman, H.L., 1948. *Natural Evaporation from Open Water, Bare Soil and Grass*, Paper Presented at Proceedings of the Royal Society of London A: Mathematical, Physical and Engineering Sciences, The Royal Society.
- Prein, A.F., Holland, G.J., Rasmussen, R.M., Clark, M.P., Tye, M.R., 2016. Running dry: the US Southwest's drift into a drier climate state. *Geophys. Res. Lett.* 43 (3), 1272–1279.
- Priestley, C., Taylor, R., 1972. On the assessment of surface heat flux and evaporation using large-scale parameters. *Mon. Weather Rev.* 100 (2), 81–92.
- Rimmer, A., Samuels, R., Lechinsky, Y., 2009. A comprehensive study across methods and time scales to estimate surface fluxes from Lake Kinneret, Israel. *J. Hydrol.* 379 (1–2), 181–192.
- Rodell, M., Houser, P., Jambor, U., Gottschalck, J., Mitchell, K., Meng, C.-J., Arsenault, K., Cosgrove, B., Radakovich, J., Bosilovich, M., 2004. The global land data assimilation system. *Bull. Am. Meteorol. Soc.* 85 (3), 381–394.
- Rosenberry, D.O., Winter, T.C., Buso, D.C., Likens, G.E., 2007. Comparison of 15 evaporation methods applied to a small mountain lake in the northeastern USA. *J. Hydrol.* 340 (3–4), 149–166.
- Rotstayn, L.D., Roderick, M.L., Farquhar, G.D., 2006. A simple pan-evaporation model for analysis of climate simulations: evaluation over Australia. *Geophys. Res. Lett.* 33 (17).
- Rui, H., Beaudoin, H., 2011. *Readme Document for Global Land Data Assimilation System Version 2 (GLDAS-2) Products*. DISC, GES.
- Sacks, L., Lee, T., Radell, M., 1994. Comparison of energy-budget evaporation losses from two morphometrically different Florida seepage lakes. *J. Hydrol.* 156 (1–4), 311–334.
- Satterlund, D.R., 1979. An improved equation for estimating long-wave radiation from the atmosphere. *Water Resour. Res.* 15 (6), 1649–1650.
- Sawaya, K.E., Olmanson, L.G., Heinert, N.J., Brezonik, P.L., Bauer, M.E., 2003. Extending satellite remote sensing to local scales: land and water resource monitoring using high-resolution imagery. *Remote Sens. Environ.* 88 (1), 144–156.
- Scanlon, B.R., Duncan, I., Reedy, R.C., 2013. Drought and the water–energy nexus in Texas. *Environ. Res. Lett.* 8 (4), 045033.
- Sheffield, J., Goteti, G., Wood, E.F., 2006. Development of a 50-year high-resolution global dataset of meteorological forcings for land surface modeling. *J. Clim.* 19 (13), 3088–3111.
- Shiklomanov, I.A., 1999. *World Water Resources and their Use: A Joint SHI/UNESCO Product*.
- Stanhill, G., 2002. Is the Class A evaporation pan still the most practical and accurate meteorological method for determining irrigation water requirements? *Agric. For. Meteorol.* 112, 233–236.
- Stannard, D.I., Gannett, M.W., Polette, D.J., Cameron, J.M., Waibel, M.S., Spears, J.M., 2013. *Evapotranspiration From Marsh and Open-water Sites at Upper Klamath Lake, Oregon, 2008–2010 Rep.* 2328-0328. US Geological Survey.
- Swancar, A., 2015. *Comparison of evaporation at two central Florida lakes, April 2005–November 2007 Rep.* In: 2331–1258. Survey, US Geological.
- Szilagyi, J., Jozsa, J., 2008. New findings about the complementary relationship-based evaporation estimation methods. *J. Hydrol.* 354 (1–4), 171–186.
- Tahoe Environmental Research Center, 2015. *Tahoe: State of the lake report.* available at: <http://terc.ucdavis.edu/stateofthelake/index.html>.
- Talley, L.D., Pickard, G.L., Emery, W.J., Swift, J.H., 2011. Chapter 5 - mass, salt, and heat budgets and wind forcing. In: Talley, L.D., Pickard, G.L., Emery, W.J., Swift, J.H. (Eds.), *Descriptive Physical Oceanography (Sixth Edition)*. Academic Press, Boston, pp. 111–145.
- Tanny, J., Cohen, S., Assouline, S., Lange, F., Grava, A., Berger, D., Teltch, B., Parlange, M., 2008. Evaporation from a small water reservoir: direct measurements and estimates. *J. Hydrol.* 351 (1), 218–229.
- Trokhimovski, Y.G., Westwater, E.R., Han, Y., Leuski, V.Y., 1998. Air and sea surface temperature measurements using a 60-GHz microwave rotating radiometer. *IEEE Trans. Geosci. Remote Sens.* 36 (1), 3–15.
- United Nations Environment Programme, 2013. *Global Environment Outlook 2000*, Routledge.
- Valiantzas, J.D., 2006. Simplified versions for the Penman evaporation equation using routine weather data. *J. Hydrol.* 331 (3), 690–702.
- van Dijk, A.I.J.M., Schellekens, J., Yebra, M., Beck, H.E., Renzullo, L.J., Weerts, A., Donchyts, G., 2018. Global 5 km resolution estimates of secondary evaporation including irrigation through satellite data assimilation. *Hydrology Earth System Sciences* 22 (9), 4959–4980.
- Vautard, R., Cattiaux, J., Yiou, P., Thépaut, J.-N., Ciais, P., 2010. Northern hemisphere atmospheric stilling partly attributed to an increase in surface roughness. *Nat. Geosci.* 3 (11), 756.
- Vining, K.C., Chase, K.J., Loss, G.R., 2013. *General Weather Conditions and Precipitation Contributing to the 2011 Flooding in the Mississippi River and Red River of the North Basins, December 2010 through July 2011: Chapter B in 2011 Floods of the Central United States, Rep* 2330–7102. Survey, US Geological.
- Walter, M.T., Wilks, D.S., Parlange, J.-Y., Schneider, R.L., 2004. Increasing evapotranspiration from the conterminous United States. *J. Hydrometeorol.* 5 (3), 405–408.
- Wang, K., Dickinson, R.E., 2012. A review of global terrestrial evapotranspiration: observation, modeling, climatology, and climatic variability. *Rev. Geophys.* 50 (2).
- Wang, W., Lee, X., Xiao, W., Liu, S., Schultz, N., Wang, Y., Zhang, M., Zhao, L., 2018. Global lake evaporation accelerated by changes in surface energy allocation in a warmer climate. *Nat. Geosci.* 11 (6), 410–414.
- Weisman, R.N., Brutsaert, W., 1973. Evaporation and cooling of a lake under unstable atmospheric conditions. *Water Resour. Res.* 9 (5), 1242–1257.
- Wild, M., 2012. Enlightening global dimming and brightening. *Bull. Am. Meteorol. Soc.* 93 (1), 27–37.
- Wild, M., 2015. Decadal changes in radiative fluxes at land and ocean surfaces and their relevance for global warming. *Wiley Interdiscip. Rev. Clim. Chang.* 7 (1), 91–107.
- Winter, T.C., 1981. Uncertainties in estimating the water balance of lakes. *JAWRA Journal of the American Water Resources Association* 17 (1), 82–115.
- Winter, T., Rosenberry, D., Sturrock, A., 1995. Evaluation of 11 equations for determining evaporation for a small lake in the north central United States. *Water Resour. Res.* 31 (4), 983–993.
- Woessner, W.W., Sullivan, K.E., 1984. Results of seepage meter and mini-piezometer study, Lake Mead, Nevada. *Groundwater* 22 (5), 561–568.
- Wolf, S., Keenan, T.F., Fisher, J.B., Baldocchi, D.D., Desai, A.R., Richardson, A.D., Scott, R.L., Law, B.E., Litvak, M.E., Brunell, N.A., 2016. Warm spring reduced carbon cycle impact of the 2012 US summer drought. *Proc. Natl. Acad. Sci.* 113 (21), 5880–5885.
- Xia, Y., Mitchell, K., Ek, M., Sheffield, J., Cosgrove, B., Wood, E., Luo, L., Alonge, C., Wei, H., Meng, J., 2012. Continental-scale water and energy flux analysis and validation for the North American Land Data Assimilation System project phase 2 (NLDAS-2): 1. Intercomparison and application of model products, *Journal of Geophysical Research: Atmospheres* 117 (D3).
- Xiao, K., Griffis, T.J., Baker, J.M., Bolstad, P.V., Erickson, M.D., Lee, X., Wood, J.D., Hu, C., Nieber, J.L., 2018. Evaporation from a temperate closed-basin lake and its impact on present, past, and future water level. *J. Hydrol.* 561, 59–75.
- Zhang, H., Gorelick, S.M., Zimba, P.V., Zhang, X., 2017. A remote sensing method for estimating regional reservoir area and evaporative loss. *J. Hydrol.* 555, 213–227.
- Zhao, G., Gao, H., 2018. Automatic correction of contaminated images for assessment of reservoir surface area dynamics. *Geophys. Res. Lett.* 45 (12), 6092–6099.
- Zhao, G., Gao, H., Naz, B.S., Kao, S.-C., Voisin, N., 2016. Integrating a reservoir regulation scheme into a spatially distributed hydrological model. *Adv. Water Resour.* 98, 16–31.